Structure Based Drug Design Considering Inhibitor-Induced Conformational Change

（阻害剤誘導によるコンホメーション変化を考慮した構造学的薬物設計）

Takayoshi Kinoshita

Osaka University
2003

Preface

I express my sincere gratitude to Professor Yasushi Kai, Department of Materials Chemistry, Graduate School of Engineering, Osaka University, for his cordial guidance, discussion and encouragement throughout the preparation of this thesis.

I am also grateful to Dr. Toshiji Tada, Osaka Prefecture University for kind and helpful suggestions.

I am indebted to Dr. Toshio Goto, Executive Director, and Dr. Takashi Fujii, Director of the Exploratory Research Laboratories, Fujisawa Pharmaceutical Co., Ltd., for giving me an opportunity to perform this study.

I thank Dr. Masahiro Neya and Dr. Isao Nakanishi of Fujisawa Pharmaceutical Co., Ltd. for helpful consultations, discussions and technical assistance, and Mr. Masaichi Warizaya and Nobuya Nishio of Fujisawa Pharmaceutical Co., Ltd. for their helpful discussions and technical assistance in the X-ray crystal structure analysis. I also thank Dr. Mitsuo Ataka of the National Institute of Advanced Industrial Science and Technology (AIST, Kansai) for helpful discussions and technical assistance in crystallization in a high magnetic field.

Special thanks are due to Dr. David Barrett, Medicinal Chemistry Research Laboratories, Fujisawa Pharmaceutical Co., Ltd., for helpful discussions and critical reading of this thesis.

Finally, I thank my parents, my wife and my daughters for their understanding, encouragement and support.

March, 2003

Takayoshi Kinoshita

Contents

Abbreviations

ADA	Adenosine Deaminase
SBDD	Structure-Based Drug Design
PPE	Porcine Pancreatic Elastase
HLE	Human leukocyte Elastase
AR	Aldose Reductase
HDPR	6-Hydroxyl-1,6-dihydropurine riboside
RMSD	Root-Mean Square Deviation
TIM	Triosephosphate isomerase
Tris	Tris(hydroxymethyl)aminomethane
HEPES	4-(2-Hydroxyethyl)piperazine-1-ethanesulphonic acid
NADPH	Nicotineamide-adenine dinucleotide phosphate (reduced)

General Introduction

In several decades, pharmaceutical companies have developed the medicines against hopeful targets by comprehensive methods with a unique philosophy and greatly expected a help from serendipity, because the phenomena in vital were obscure. Thus, slow development of the drugs had been allowed because of no competition. Recently, human genome has been clarified and thus the phenomena in vital have become apparent successively. Therefore, many companies tend to concentrate on similar targets, however, only companies that produce effective drugs as fast as possible can survive the intense competition. As an effective method for the demand of haste development, Structure-Based Drug Design (SBDD) has been used all over the world. SBDD is defined as rational design based upon careful investigation of the crystal structure of the complex of the target protein and its inhibitor. Using SBDD, the number of the compounds necessary for examination of a working hypothesis can be reduced dramatically. Consequently, the shortened period to produce drug entities enables a company to survive the severe competition.

However, SBDD has a number of problems. First, crystallization of the target-inhibitor complex is difficult and time-consuming. For successful SBDD, it is important to speed up this critical step and to shorten the harvest period of high-quality crystals. Second, protein has infinite number of conformations in the active site. Generally, protein has an open-close motion in order that substrate and/or inhibitor binds to and leaves the active site. Nevertheless, general SBDD has been performed using a static structure up to this point. Thereby, behaviors of designed compounds have often disagreed with that as we pleased.

For overcoming the technical problem, I have modified the crystallization method of a target protein, which can be applied to other proteins. Furthermore, I would like to devise the new SBDD considering the inhibitor-induced conformational change through studies on three target proteins, adenosine deaminase, aldose reductase and pancreatic elastase.

1. Adenosine Deaminase

1-1 Introduction

Adenosine deaminase (ADA, EC 3.5.4.4) has a zinc atom at the center of the active site and catalyzes the irreversible deamination of both adenosine and deoxyadenosine to inosine and deoxyinosine, respectively (figure 1-1). ADA is one of the enzymes involved in the purine pathway and is distributed in most mammalian tissues. It is indispensable to the upkeep of a competent immune system, since heritable deficiency of ADA is associated with severe combined immunodeficiency disease (SCID) [1]. ADA has also been shown to be involved in T cell activation [2]. Both enzyme replacement therapy [3] and gene therapy [4] have been used to treat victims of this rare disease. On the other hand, higher levels of ADA are associated with a number of diseases and ADA inhibitors have seen clinical usage as antimetabolic and antineoplastic agents and as modulators of neurological function through their effects on adenosine levels [5,6]. However, these drugs are seldom used because of severe toxicity resulting from the fact that all known inhibitors are nucleoside analogues. Therefore, toxicity-free drugs would be a major and significant improvement.

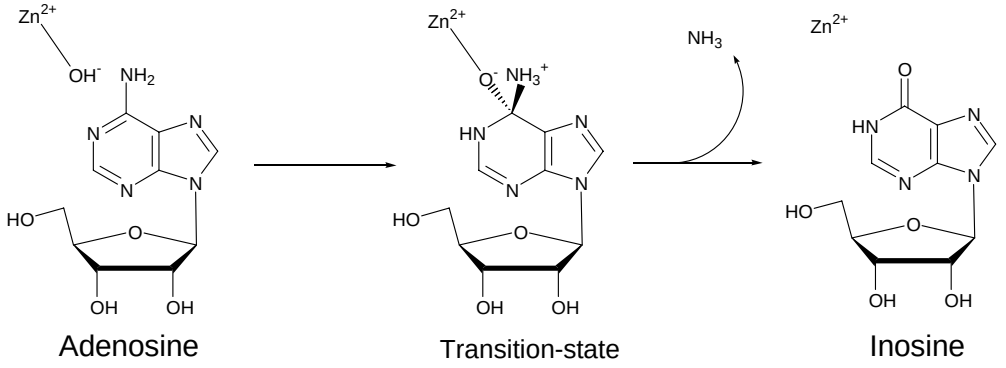

Figure 1-1. Reaction mechanism of adenosine deaminase. Water activated by the zinc attacks the C-6 carbon of adenosine to form a transition-state. Ammonia leaves out from the transition-state and inosine is generated.

For the purpose of discovery of improved drugs, structure-based drug design (SBDD) with the aim of discovery of the non-nucleoside inhibitors may be most effective. As the first step of SBDD, we planned to examine human ADA by X-ray analysis, however, sufficient quantities of human ADA was difficult to obtain. We thus decided to examine bovine ADA, although all X-ray studies to date on ADA have been carried out using mouse ADA [7-11].

Bovine ADA is the closest to human ADA amongst known ADA amino acid sequences. Furthermore, bovine ADA derivatized with polyethylene glycol [12] has been administered to replace deficient human ADA. This means that human and bovine

ADA are very close to each other and are functionally interchangeable. The amino acid sequences of human and bovine ADA are 91% homologous [13,14]. Bovine and mouse ADA [15] are 85%, and human and mouse ADA are 83% homologous, respectively. In particular, the amino acid residues around the active sites of human and bovine ADA are completely identical.

Furthermore, it is suggested that the active sites of bovine ADA and human ADA are different from that of mouse ADA, since a single mutation is present at a structurally important site, namely at the end of the movable component of the active site cleft. ADA has a common structural motif, a TIM-barrel which contains a parallel α/β-barrel motif with eight central β-strands and eight helices, and which has movable components on the top of the barrel. These types of components often move greatly if an inhibitor or substrate binds to the active site. For example, aldose reductase and triosephosphate isomerase have different conformations as a result of inhibitor-induced fitting when inhibitors bind [16,17].

We believe that precise observation of the structural features of bovine ADA may lead to the design of novel non-nucleoside type inhibitors, which may be safe drugs, due to functional and structural similarity to human ADA. For that purpose, the crystal structure of bovine ADA complexed with two different types of inhibitors, FR117016 and HDPR[1] (figure 1-2), are analyzed in detail.

FR117016 was found out from random screening using the chemical library of our company. It had inhibitory activity with a Ki value[1] of 1.2 μM against recombinant human ADA and 0.7 μM against bovine ADA. On the other hand, HDPR is a well-known and nucleoside analogue. FR117016 is quite different from substrate derivative such as HDPR.

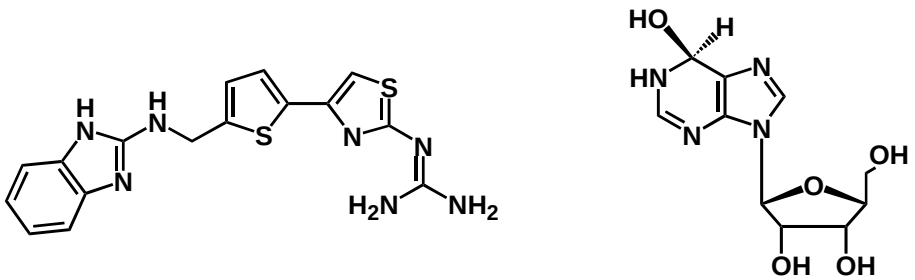

a)FR117016 b)HDPR

Figure 1-2. Chemical structures of ADA inhibitors. a) FR117016. b) HDPR: 6-hydroxyl-1,6-dihydropurine riboside. The structure of FR117016 is novel and quite different from substrate derivative inhibitors such as HDPR.

[1] Ki value: Inhibition value. The value indicates the extent of inhibition. Smaller value indicates the stronger inhibition. Ki = [E][I]/[EI].

1-2 Material and methods

1-2-1 Crystallization

ADA from bovine intestine was purchased from Boehringer-Mannheim Biochemicals, and purine riboside from Sigma. The protein solution used with no further purification for the crystallization was at 20 mg/ml in 50 mM Tris-HCl buffer at pH 7.5 with 10 mM purine riboside. All trials of the crystallization were carried out by the hanging drop method of vapor diffusion by mixing 2 μl of bovine ADA protein solution with 2 μl of the reservoir solution and equilibrating the drops over the reservoir at room temperature. First trail was done using grid sceening based on the condition for the crystallization of mouse ADA: 15% (w/v) polyethylene glycol 6000, 0.1M citrate buffer at pH 4.2 [18]. But, those experiments did not yield any crystals but amorphous aggregation. Additional trials were performed using a commercially available sparse matrix screening kit from Hampton Research [19]. Small crystals of the complex with purine riboside were obtained from the experiments designed on the basis of results from the screening. The crystals of bovine ADA complexed with purine riboside used for data collection were grown against reservoirs containing 2.0 - 2.2 M ammonium sulphate, 2% (v/v) polyethylene glycol 400 in 0.1 M HEPES buffer at pH 7.5. The crystals of both complexes grow to maximum dimensions of approximately 0.3 x 0.2 x 0.15 mm in two weeks.

1-2-2 Modification of crystallization for smooth SBDD

The quality of crystals is very important for determining the precise structure for structure based drug design (SBDD), one of the most powerful processes for producing effective drugs. Accurate and reliable structures are available when X-rays diffract to higher resolution in all directions. Therefore, a number of more or less general means to improve the quality of protein crystals in the course of crystal growth are being developed. At present, methods to increase the stability of the crystal growth environment include growth in a high magnetic field [20], growth with gels [21-23], growth in microgravity [24], and growth in the presence of cross-linked agents [25].

A further important requirement is that the harvest period for obtaining crystals must be sufficiently short for a smooth and efficient SBDD cycle. A complex with a new class of inhibitor must be analyzed within 2 weeks to 1 month, since other investigations, except for X-ray analysis, can usually be finished within 1 month. To obtain effective drugs, a number of SBDD cycles are necessary. Therefore, speedy acquisition of complex crystals will assist the successful SBDD.

We have already shown that crystals of bovine adenosine deaminase (ADA) are

easily grown in the presence of an inhibitor in two weeks. However, most of the crystals were of relatively low quality with a large amount of brown sticky precipitation in the normal environment. Only 5% of all crystals grown could be used to collect diffraction data. On the other hand, using the other 95% of the crystals, data could not be measured because diffraction spots were streaked or split. Moreover, even a large crystal scarcely diffracted to over 2.5 Å resolution.

To supply precise information for SBDD timely and successively, higher resolution structures must be determined in a short time. Thus, methods to improve the quality of crystals must be developed, maintaining or reducing the harvest period of the growth. In our present example with bovine ADA, the harvest period of two weeks was acceptably short for SBDD. However, since crystal quality was generally poor in most batches, we could not carry out SBDD effectively without some means to improve the crystal quality. We therefore tested two alternative environments. One was crystallization with agarose gel, which can be used easily and is most popular. The other was crystallization in a magnetic field, which has recently been shown to improve the quality of certain protein crystals [20]. It was assumed that a magnetic field would be useful for ADA since it may have a high dipole moment based upon architecture involving the α,β-barrel motif and zinc on the top of the barrel. We compared crystals grown in the three environments to establish the optimum conditions for SBDD.

Bovine ADA was purchased from Roche Diagonostics Inc. and used without further purification. Thus far, several lots of commercial ADA were characterized to be almost identical in solution, based upon checking by means of SDS-PAGE, dynamic light scattering and enzymatic activity. Moreover, all crystallization experiments lead to the same results. Purine riboside as a potent inhibitor and agarose gel (type V: high gelling temperature) were purchased from Sigma. ADA crystals were prepared by the sitting-drop vapor diffusion method in all environments studied. All operations were carried out in a temperature-controlled laboratory (293±2 K) using crystallization plates with 24 chambers purchased from the Charles Supper Company.

As a control, we used crystals grown outside the magnetic field and without agarose gel. The procedure for crystallization described in detail before was modified in order to eliminate experimental differences. First, 4 μl drops of the sample buffer, 25mM Hepes at pH 7.5, were placed on the sitting basin in the centre of the wells. Subsequently, 4 μl drops of the reservoir solution and 8 μl drops of the protein solution were mixed with the sample buffer already set up. Crystallization with agarose gel was performed using the same procedure as the control, except that agarose gel was added to the sample buffer. The concentration of agarose gel was optimized to 0.1 % (w/v), a concentration

at which the solution was highly viscous. The procedure for crystallization in a magnetic field was also performed in a similar manner as the control. Immediately after making the crystallization drops, wells were inserted into a temperature-controlled bore (293±1 K) of a liquid helium-free superconducting magnet (JASTEC) at National Institute of Advanced Industrial Science and Technology (AIST Kansai). The bore was 100 mm in diameter and oriented vertically. The plates were fractionated to the 4 wells due to the bore size. The fractionated container was placed at the position of maximum field (the centre of the magnet). Crystals were grown under a homogeneous and static magnetic field of 10 T. The container was placed in a temperature-controlled incubator (293±0.5 K) for a few days until data collection.

All crystals, selected with points of the same size as possible, were dipped into a solution of NVH oil (Hampton Research Inc.) before data collection. The crystals were also placed in the x-ray stream with a similar orientation. Optical microscope observation and photographs were used to evaluate the size and orientation of crystals. For equal comparison, diffraction data sets were collected on an R-AXIS VI^{++} image plate on a RIGAKU rotating anode generator operated at 50 kV and 100 mA. This source is rather weak and inferior but can provide a constant X-ray in terms of intensity compared with synchrotron sources. For example, at the synchrotron source at SPring-8/BL24XU, the intensity decays more than 20 % per 12 hr. For exact comparison, common experimental parameters were used. Each of the 1.0 $^{\circ}$ oscillation images were exposed for 15 minutes. The distance of crystal-to-image was 100 mm. The total oscillation ranges of the respective data sets were decided according to indications from the program Crystal Clear (RIGAKU) in order to have the same redundancies with 99 % completeness. Data were also processed with Crystal Clear. The statistics of the crystallization and data collection are shown in table 1-1.

Most crystals grown as the control had poor shapes (figure 1-3a) and their diffraction spots were streaked or split (figure 1-4a). Only one batch among the twenty batches we prepared for our structure determination had a high-quality crystal with clear edges, and it diffracted to 2.5 Å resolution. The crystal used for data collection grew within 2 weeks and had appropriate dimensions of $0.20 \times 0.15 \times 0.15$ mm^3. In almost all batches, 5-10 crystals per batch emerged with a large amount of additional brown precipitation. The optimum concentration of ammonium sulphate as a precipitant was 2.0-2.1 M.

In the crystallization with agarose gel, the probability of obtaining high-quality crystals was somewhat increased compared with the control. Furthermore, brown precipitation was decreased because the random aggregation of protein molecules may be suppressed. Generally, aggregation judged by a character test such as dynamic light

scattering almost always leads to precipitation. All batches prepared contained 1-5 crystals. Five out of ten batches prepared had good crystals. A poor shaped crystal is shown in figure 1-3b, and a well-shaped one in figure 1-3c. The good shaped crystals had clear edges, diffracting to 2.2 Å resolution with dimensions of 0.30 × 0.20 ×0.20 mm^3. However, the harvest period necessary to obtain a crystal as in figure 1-3c was extended to 1 month. We assume that this elongation results from the role of the agarose gel to control molecular motion in solution. In other words, agarose gel suppresses crystal nucleus formation as well as crystal growth. The slow growth leads to suppression of random aggregation and also to improvement of the crystal quality. The optimum concentration of ammonium sulphate as a precipitant was slightly increased to 2.1-2.2 M. In agreement with the previous arguments [21], we could demonstrate the superiority of the gel environment, but also experienced its limitation for SBDD in terms of the speed of obtaining high-quality crystals.

Finally, in the crystallization in a high magnetic field, the probability of obtaining high-quality crystals was greatly increased. Brown precipitation was completely inhibited since random aggregation was totally suppressed in the magnetic field. All batches contained good crystals. The crystals had clear edges (figure 1-3d), diffracted to 2.0 Å resolution with sharp and clear pattern (figure 1-4b) and had dimensions of 0.30 ×0.20 ×0.20 mm^3. Furthermore, the harvest period of the crystals was reduced to 9 days, much shorter than in the case of using gel. One to three crystals per batch emerged in every experiment. With the precipitant concentration used for the control- and gel-experiments of 2.0-2.2 M ammonium sulphate, no crystal was obtained in a magnetic field. The optimum concentration of ammonium sulphate was found to be much higher, i. e. 2.3-2.4 M. At this concentration, in the control- and gel-environments, many tiny crystals, inappropriate for structure determination, were obtained within about 1 week. Since the magnetic field strongly suppressed both the formation of crystal nuclei and precipitation, it is thought that the higher concentration of ammonium sulphate could effectively promote the crystal growth within a short period.

It was shown that both agarose gel and a magnetic field improved the quality of ADA crystals to a greater extent than expected at the beginning of this work. Both environments were favorable to crystal growth of ADA based on the data shown in table 1-1. From a practical viewpoint, crystallization in a magnetic field gave a higher yield of high-quality crystals without brown precipitant. Furthermore, magnetically grown crystals diffracted to higher resolution than control- and gel-crystals. A magnetically grown crystal diffracted to 2.0 Å resolution, and a gel-crystal to 2.2 Å

when the same sized crystals were used. Therefore, the magnetic field improved most effectively the crystal quality.

Additionally, crystals in a magnet could be obtained in the shortest period among the three environments. Generally, it may be expected that the agarose gel delays the harvest period because of the suppression of forming crystal-nuclei and molecular motion in the gelled environment. In fact, the gel-crystal grew in 1 month or more. Sometimes, crystal growth in a magnetic field is reported to be slower than the control [26]. In our case also, the magnetic field slowed down crystal nucleation, however, increasing and optimizing the precipitant concentration could compensate for this, and our crystals grew within 9 days without any detrimental side effects.

We therefore conclude that we could achieve our goal of sufficiently rapid growth of high-quality crystals of ADA by employing crystal growth in a magnetic field. Note that the resolution given here can still be improved, and that the harvest period can also be shortened more, since a smaller crystal can provide the necessary resolution for structure analysis, if synchrotron radiation is used as the X-ray source.

Table 1-1. Crystallization and preliminary crystallographic data of ADA crystals in three environments.

	Control	Agarose gel	Magnetic field
Crystallization			
Optimum precipitant concentration	2.0-2.1 M	2.1-2.2 M	2.3-2.4 M
Time	2 weeks	1 month	9 days
Average crystal size (mm)	0.20 x 0.15x 0.15	0.30 x 0.20 x 0.20	0.30 x 0.20 x 0.20
Number of crystal per batch	5-10	1-5	1-3
Number of high quality crystals	1/20	5/10	6/6
X-ray data collection at 100 K			
Unit cell parameters (Space group $P4_32_12$)			
a (Å)	77.19	77.30	77.22
c (Å)	135.62	135.58	134.90
Diffraction limit (Å)	2.5	2.2	2.0
$I/\sigma(I)$ overall	10.5	7.7	9.6
$I/\sigma(I)$ in the highest shell	3.4	3.1	3.3
Rmerge overall (%)	5.0	6.8	6.6
Rmerge in the highest shell (%)	18.7	26.4	21.6
Completeness overall (%)	99.2	98.8	99.1
Completeness in the highest shell (%)	99.9	99.1	98.1

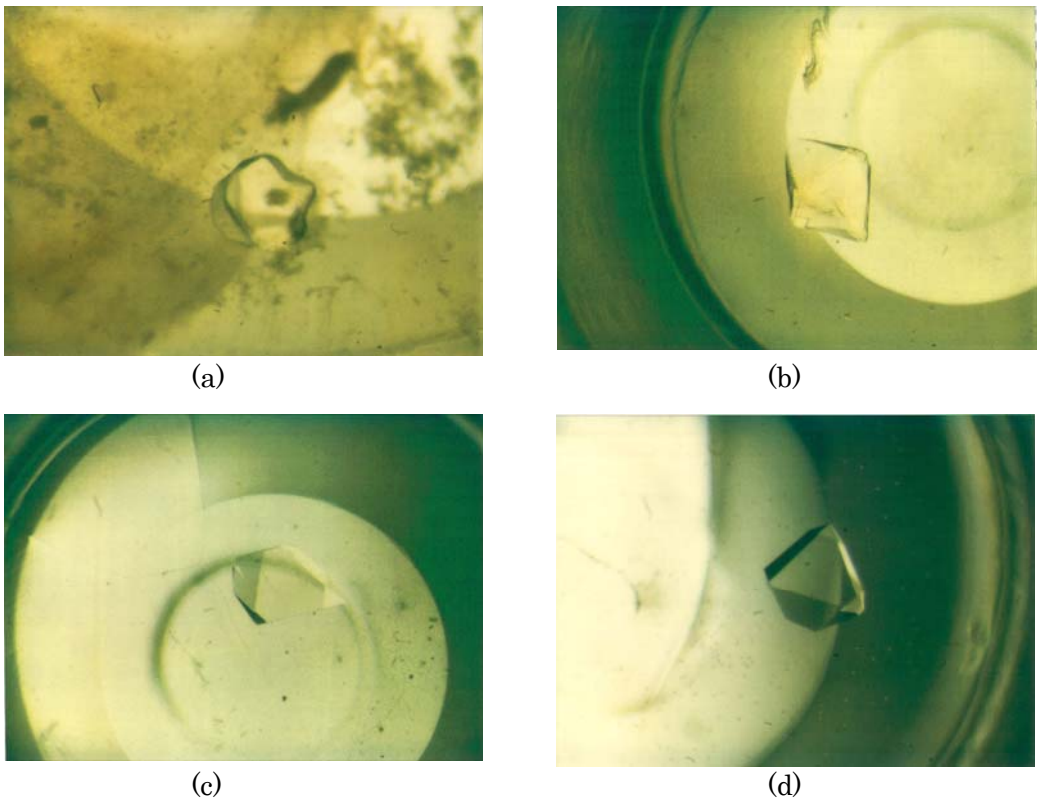

Figure 1-3. Photographs of ADA crystals prepared under several environments. (a) A typical crystal in the control environment without a gel or a magnetic field. Crystals with poor edges emerged with a large amount of additional brown precipitation. (b) A poor crystal grown in agarose gel. A crystal having poor edges emerged with a small amount of brown precipitation. (c) A good crystal that grew in an environment with agarose gel. (d) A crystal in a magnetic field. Under 10 T magnetic field, all crystals in all batches had sharp edges. Furthermore, no precipitation occurred. They diffracted to a resolution of 2.0 Å.

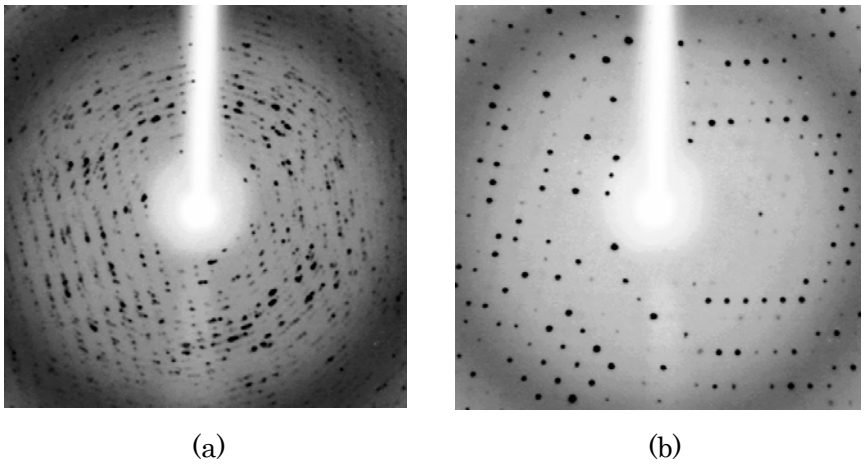

Figure 1-4. Diffraction images from ADA crystals we investigated within 4 Å resolution. (a) An image from a typical crystal in the control environment. The diffraction spots were streaked. (b) An image from a good crystal. The diffraction spots were sharp and clear.

1-2-3 Data collection

After dipping a crystal in a solution of Paratone-N (Hampton Research Inc.), X-ray diffraction data were collected at 100 K using a Rigaku R-AXIS V imaging-plate system at the beam line BL24XU of a SPring-8 facility (Harima, Japan). The crystal-to-imaging plate distance was 300 mm and the oscillation range was 1 degree with exposure time of 30 sec. The image was up to 150 frames. The data processing was performed using program Crystal Clear (Rigaku). The data-collection statistics for the data set are summarized in table 1-2.

1-2-4 Structure determination

The structure of the complex was solved by the molecular replacement technique-using program AMoRe from the CCP4 program suite [27]. At first, the structure of mouse ADA [7], registered as the code 1ADD in the Protein Data Bank, was directly used as a search model. However, this attempt did not lead to a clear solution. Therefore, the model of bovine ADA was used as a search model. This homology model was constructed based upon the crystal structure of mouse ADA using SYBYL molecular modeling software (Tripos Inc). The model was energetically minimized to avoid illegal contacts. The rotation function successfully afforded a clear solution. Subsequently, a clear solution of the translation function was obtained in the case of space group $P4_32_12$ and no illegal contacts in the crystal were detected. Furthermore, the electron density of the helix part showed a precise α-helix. Thus, the space group of the crystal was confirmed to be $P4_32_12$.

After a subsequent rigid-body refinement, HDPR and FR117016 were easily placed in the 2 σ level envelope of the $|F_{obs}| - |F_{calc}|$ difference map. Subsequently, a refinement with all data was performed in the CNX package (Accelrys Inc.) using torsion angle dynamics and individual B-factor refinement. A randomly selected 5 % of the data set was set aside for cross-validation using the R_{free} value and bulk-solvent correction was used. During the refinement, solvent molecules were progressively added when they met the following requirements: (i) a minimum 3 σ peak had to be present in the $|F_{obs}| - |F_{calc}|$ difference map, (ii) a peak had to be visible in the $2|F_{obs}| - |F_{calc}|$ map, (iii) the B value for the water molecule should not exceed 80 $Å^2$ during refinement and (iv) the water molecules had to be stabilized by hydrogen bonding. Visual inspection and model building were performed using Quanta (Accelrys Inc.).

Table 1-2. Data collection and refinement statistics of HDPR complex and FR117016 complex

	HDPR complex	FR117016 complex
Data collection and processing		
Unit cell parameters		
a, *c* (Å)	79.19, 141.62	78.03, 136.66
Diffraction data		
Resolution (Å)	30.0 - 2.5	30.0-2.3
Unique reflections	16108	18880
Rsym (%)	5.0(18.7)	6.7(27.8)
Completeness (%)	99.2(100.0)	97.2(99.9)
Redundancy	8.9(7.9)	9.5(9.3)
$I/\sigma(I)$	10.5(3.4)	7.2(2.4)
Refinement		
Rcryst/Rfree (%)	20.7/24.1	22.5/25.7
Final model		
Protein residues	349	349
Zn^{2+}	1	1
HDPR/FR117016	1	1
Water	222	458
R.M.S. diviations		
Bonds (Å)	0.007	0.036
Angles (degrees)	1.6	5.0
Dihedrals (degrees)	24.3	26.8
Mean B factor ($Å^2$)		
Protein	42.9	44.4
Zn^{2+}	26.6	61.1
HDPR	27.9	30.0
Water	56.9	59.9
All	43.9	46.7

Values in parentheses are fore the highest shells (HDPR complex: 2.59-2.50 Å, FR117016 complex: 2.35-2.30 Å).

1-3 Structure of HDPR complex

The Cα backbone traces of bovine and mouse ADA are very close to each other with an RMSD (root-mean-square deviation) value of 0.57 Å (figure 1-5), although mouse ADA could not lead to a perfect solution by molecular replacement.

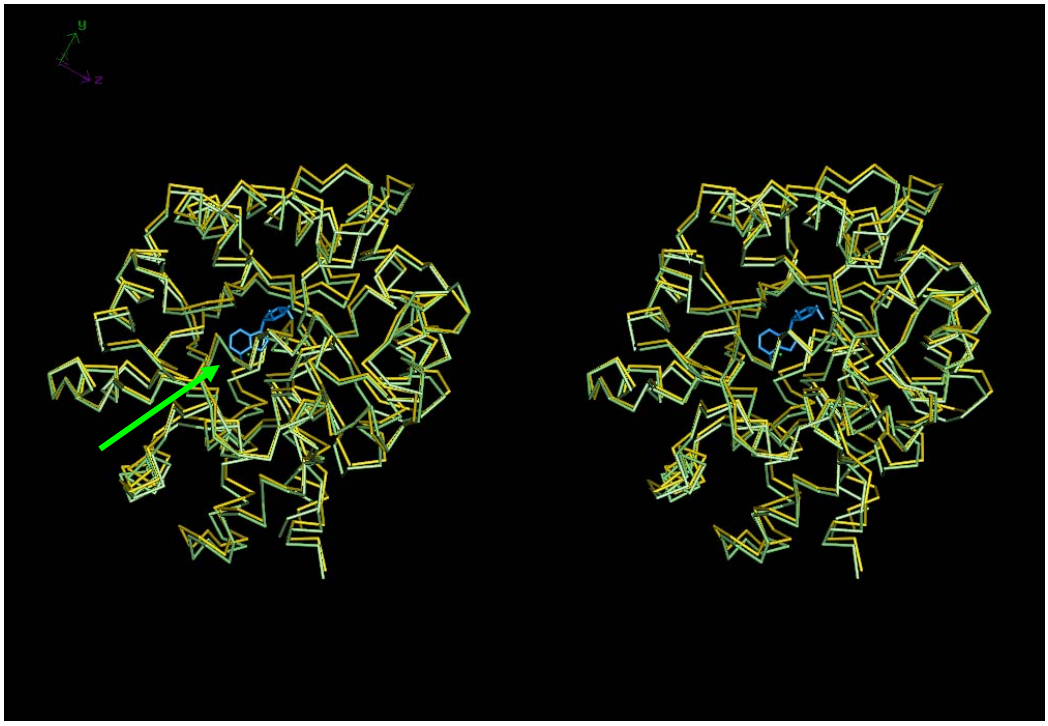

Figure 1-5. A stereo view of superimposed α-carbon backbone structures of the complex with HDPR (bovine holoenzyme: white; mouse holoenzyme: yellow; HDPR: blue). The two-holoenzyme molecules have almost the same backbones. A critical mutation is located at the top of the active site (green arrow).

The reason may be different crystal packing results in a slight, but significant, conformational change. Generally, the modification of the start model, such as a polyalanine model or an omit-model without outer region loops, can lead to a clear solution. However, the bovine ADA model was easily be constructed, rather than by modification of mouse ADA, therefore, the bovine ADA model was used as a start model. The main structural architecture of bovine ADA, the so-called TIM-barrel, remained. Two amino acids from the N-terminus and five from the C-terminus were omitted from the final model because of ambiguous or discontinuous electron density for the corresponding regions. Furthermore, the C-terminus and N-terminus in the final model lay in the solvent region and the B-factor values of the corresponding Cα atoms are high compared to the average. Thr1: 65.6, Arg349: 70.3, and average: 42.9 $Å^2$, respectively. However, the two termini of ADA are considered irrelevant to drug design since they are far removed from the putative active site.

The purine riboside was used as an inhibitor in the preparation of the complex solution, and was converted to HDPR, a hydroxyl derivative, by ADA during crystallization (figure 1-6). Furthermore, HDPR remains in the active site because of having no leaving group.

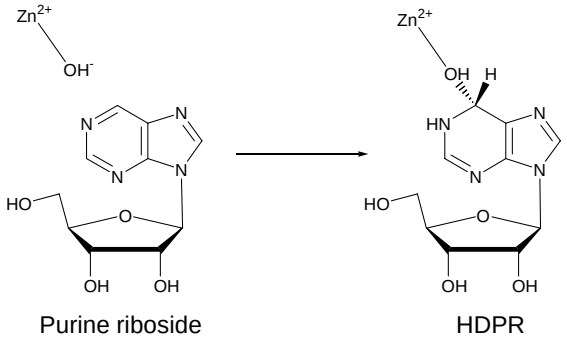

Figure 1-6. A diagram shows conversion of inhibitor. Purine riboside converted to HDPR of the 6-hydroxyl derivative. In the native ADA, activated water ligates to zinc atom. That water on the vertical direction of purine ring attacks the substrate (or a class of inhibitor). HDPR remains in the active site in the same manner of transition-state because HDPR have no leaving group on the C-6 carbon.

Subsequently, HDPR remained at the active site and formed a co-ordination bond with zinc, although the substrate adenosine converts to inosine, a hydroxyl derivative, and leaves the active site. The electron density of the inhibitor quite clearly continued from the hydroxyl group in the axial position of C-6 of the purine ring system to the zinc ion (figure 1-7). The hydroxyl group is one of the five ligands and the distance between the zinc ion and hydroxyl group of HDPR is 2.1Å. In the native structure, an activated water molecule co-ordinates to the zinc ion in place of the hydroxyl group. In addition to the hydroxyl group, the zinc ion is also co-ordinated by His12 Nε (2.2Å), His14 Nε (2.1Å), His211 Nε (2.2Å), and Asp292 Oδ1 (2.3Å). HDPR also tightly interacts with ADA by means of six hydrogen bonds (figure 1-8). The N-1 atom of the purine ring makes a hydrogen bond with Glu214 Oε (2.9Å), the N-3 atom with Gly181 NH (3.0Å), the N-7 atom with Asp293 Oδ (2.8Å), the 6-hydroxyl group with Asp292 Oδ (2.7Å), the 5'-hydroxyl group with His14 Nε (2.9Å), and the 3'-hydroxyl group with Asp16 Oδ (2.5Å). HDPR also forms a hydrogen bond directly with a water molecule in the hydrocarbon part, where water locates and this closes the entrance of the active site. 2'-hydroxyl and 3'-hydroxyl groups interact with water569 (2.7Å and 2.8 Å, respectively).

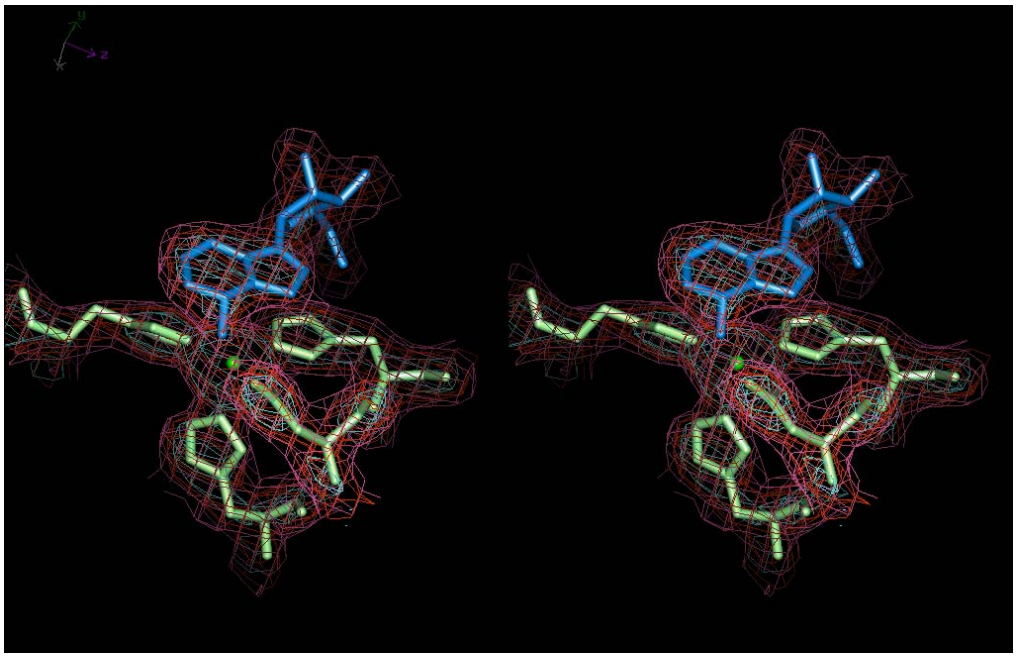

Figure 1-7. Stick models of HDPR (blue) and four amino acids (white) and a sphere model of zinc (green). The models are enclosed in the wire-cage representation of the electron density map calculated at 2.5 Å resolution by a Fourier transform using $2|Fo|-|Fc|$ as coefficients (1 σ level: pink, 2σ level: orange, 3σ level: grey). *Fc* values calculated from the final protein structure without HDPR. The electron density is continuous from the hydroxyl group in the axial position of the C-6 of purine riboside to the zinc ion. The side chains of three histidine residues and an asparagine residue on the top of TIM-barrel also make co-ordination bonds to the zinc ion.

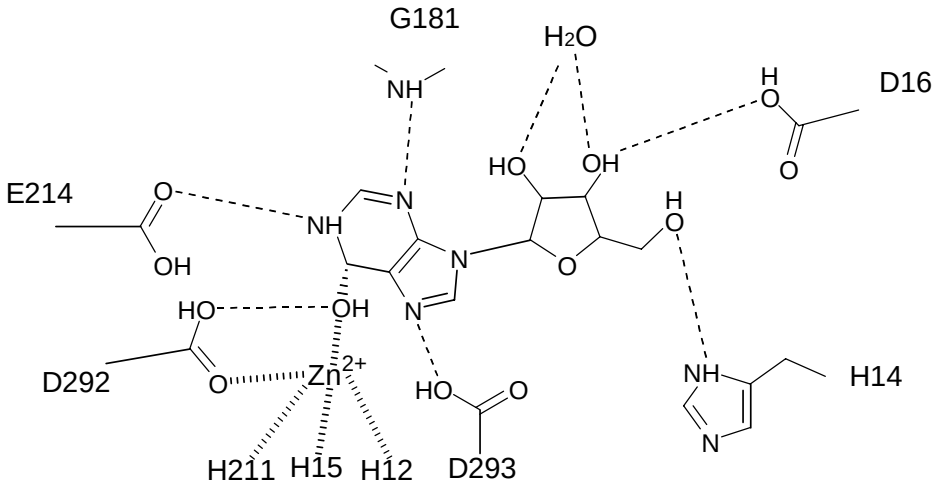

Figure1-8. Interaction mode between ADA and HDPR. The dot lines and bold dot lines show hydrogen bonds and co-ordination bonds, respectively. HDPR interacts with ADA by six direct hydrogen bonds and with zinc by a co-ordination bond. Only a water molecule interacts with HDPR by two hydrogen bonds.

Bound HDPR occupies almost the entire active-site cavity at the top of the β-barrel. The bound inhibitor is almost buried in the active site and has an accessible surface area of 8.5 $Å^2$, 3.4% of the total surface area of the unbound inhibitor (figure 1-9). Therefore, it is necessary for ADA to undergo conformational change at the active site when the inhibitor or substrate binds or leaves, since the compounds can not leave through a narrow hole around the hydrocarbon moiety of HDPR. The lid of the envelope consists of two components: one contains two leucine residues and the other contains the backbone of the opposite side. The Cδ1 atom of Leu55 interacts with the peptidyl N atom of Asp182 perpendicularly. Similarly, the Cδ2 atom of Leu59 interacts with the peptidyl N atom of Glu183. Both Cδ atoms of the two-leucine residues are 3.5 Åfrom the respective N atoms of the backbone. These weak interactions, which are similar to CH-π interactions, might make it possible to open the lid. However, the mobility of components in the crystals was undetected. In the crystal, the movable components of both types of ADA are stabilized due to inhibitor binding. Actually, the B-factors of the individual atoms of the two components are almost equivalent to the average value of all protein atoms in both ADA molecules.

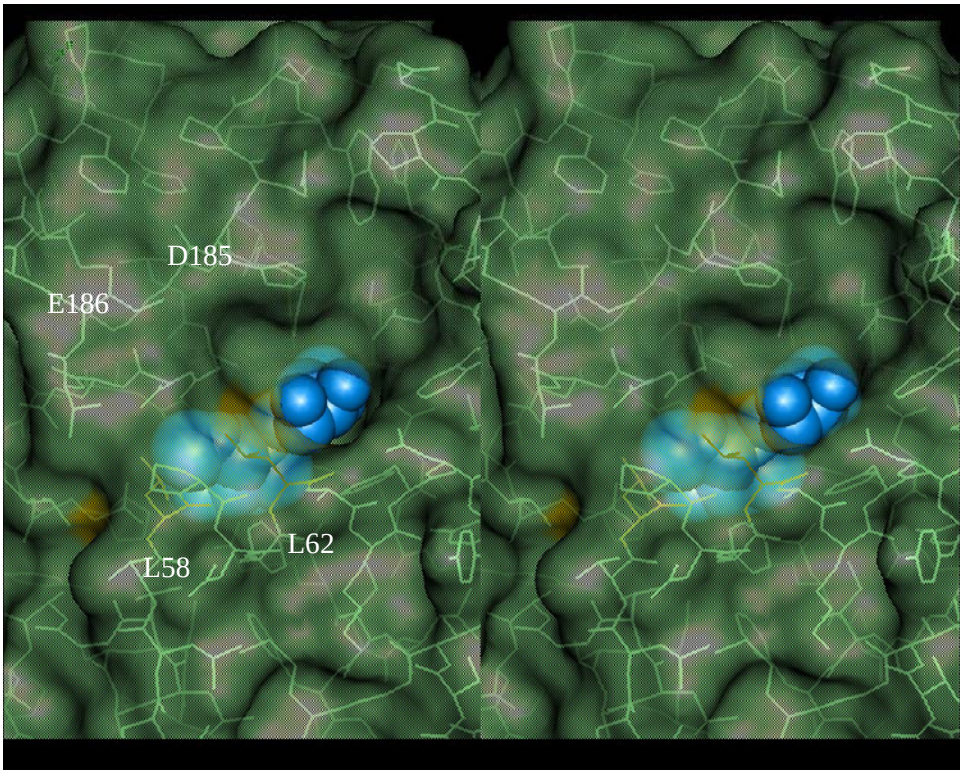

Figure 1-9. A stereo view of the movable lid. Two leucine residues (yellow) interact with the backbone N atom in the vertical direction. The interaction manner is a kind of CH-π interaction. Both of terminus C atoms are 3.5Å distances to the N atoms. Mutation site (green) is located between the significant two leucine residues. Bound HDPR (blue sphere model) is almost buried in the active site.

1-4 Structure of FR117016 complex

The backbone structures of ADA in the HDPR and FR117016 complexes are similar to each other, with an r.m.s.d. value of 1.24 Å (figure 1-10). In both complexes, ADA perfectly retains the so-called TIM-barrel motif, which contains a parallel α/β-barrel motif with eight central β-sheets and eight α-helices [28]. Generally, this motif has a flexible portion on the top of the barrel, which moves largely when an inhibitor or substrate binds to the active site. For example, aldose reductases (ARs) have several conformations around the flexible portions while they have a common conformation concerning the TIM-barrel structural motif in various complexes [29-32].

By analogy with AR, an intermediate of the open-close movement around the active site is shown in ADA. In the FR117016 complex, the helix 57-73 extends straight to the solvent region. On the other hand, in the HDPR complex, the helix 57-73 is largely bent at Phe65, the middle of the component. The simple conformational difference of the sole amino acid results in a dramatic change in the active site shape. A novel recognition site emerges, in addition to the well-known active site observed in complexes with substrate-derived inhibitors such as the HDPR complex (figure 1-11). The additional spaces consist of a thin planar hydrophobic subsite (F1) and another wide hydrophobic subsite (F2) at right angles to F1. Whereas in the HDPR complex, and other complexes, the space of the active site is completely enclosed by the lid motif consisting of two side chains of Leu58 and Leu62 and the backbone atoms of Glu186 and Asp185 (figure 1-12). The thiophene and thiazole moieties of FR117016 fit in the lid, namely the F1 site. Thus, the thiophene moiety is sandwiched by the lid motif, and they form a CH-π-π interaction. The thiophene moiety forms a CH-π interaction with Cδ of Leu62 and forms a π-π interaction with the backbone atom of Asp185. Consequently, in the FR117016 complex, the thiophene moiety elongates the width of the lid, which directly interacts in the HDPR complex (figure 1-9). The distances between Cδ of Leu62 and NH of Asp185, one of the pairs forming the lid, are 7.5 Å and 3.5 Å in the FR117016 and HDPR complexes, respectively. On the other hand, the benzimidazole moiety of FR117016 occupies the hydrophobic F2 site, which is fully occupied by the side chain of Leu58 in the HDPR complex. A large portion of FR117016 uses perfectly the new hydrophobic spaces, and only the guanidyl group uses the well-known active site forming two hydrogen bonds with Asp293, a significant residue in recognizing the substrate (figure 1-13). In the active site, important residues for substrate recognition ligate the water molecules. Therefore, this binding mode could not be predicted by a computational method without the X-ray experiment.

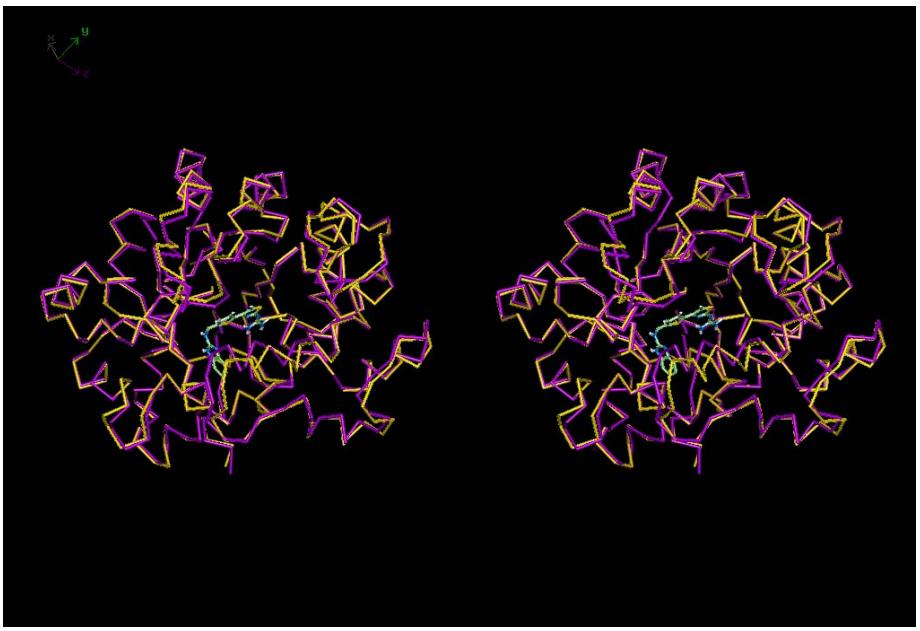

Figure 1-10. A stereo view of superimposed Cα backbone structures of the FR117016 complex (yellow stick model, holoenzyme; stick model, FR117016) and of HDPR complex (purple stick model, holoenzyme). The two holoenzymes have almost the same backbones, except for the lid of the active site. If ADA does not move in FR117016 binding, the ADA holoenzyme will overlap FR117016. In this figure, FR117016 contacts the HDPR complex shown as purple stick model.

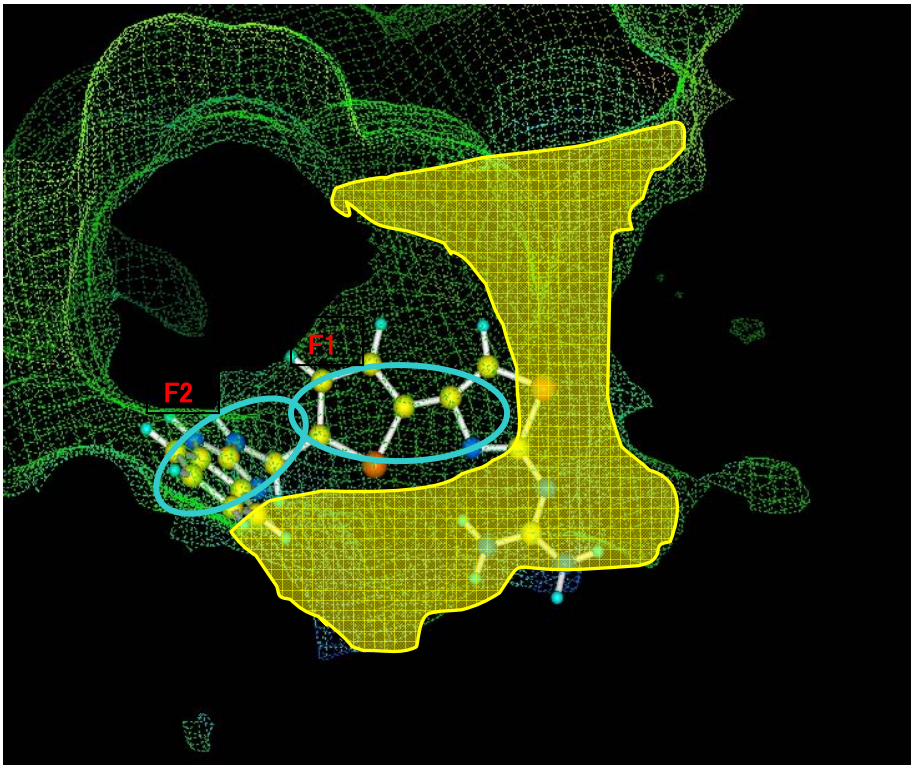

Figure 1-11. Active site envelops. The active site of HDPR complex shows as a yellow envelop. The active site envelope of FR117016 complex also shows as a green envelope. A novel recognition site emerges in addition to the well-known active site. The well-known active site such as the HDPR complex is completely conserved in the FR117016 complex. The yellow envelope is superimposable on the green envelope. On the other hand, the new site consists of a thin hydrophobic subsite (F1) and another hydrophobic subsite (F2) at the right angles to the F1 subsite. The thiophene and thiazole moieties occupy the F1 subsite and the benzimidazole moiety occupies the F2 subsite, respectively.

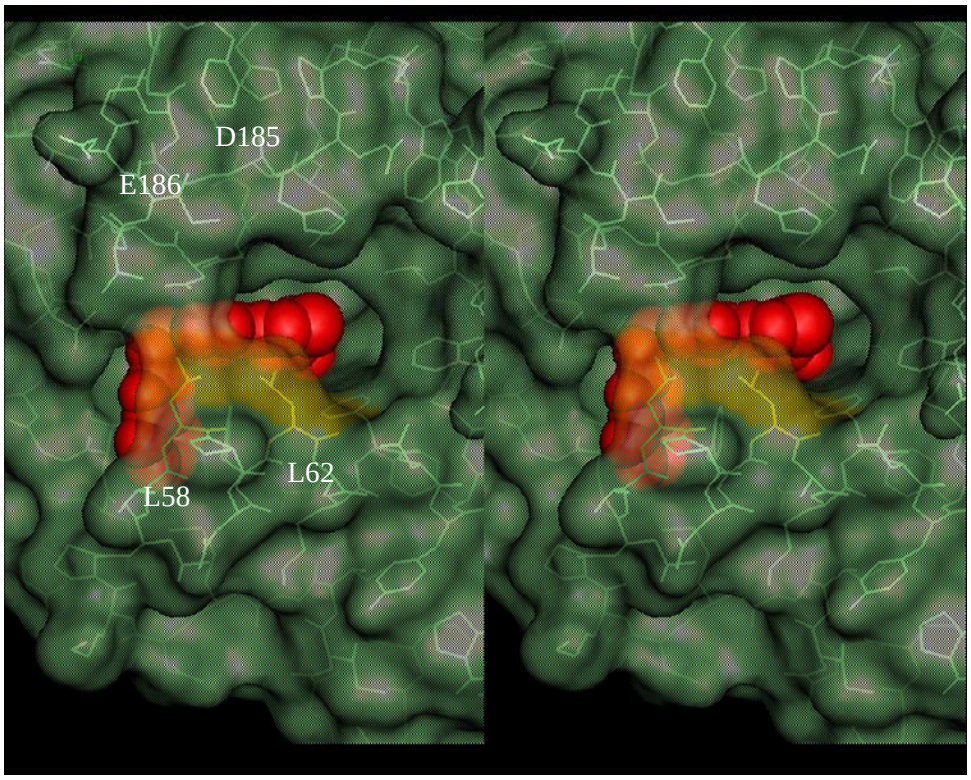

Figure 1-12. Stereo view of the top surface at the active site in the FR117016 complex. The active site shapes of two complexes are different from each other (compared with Figure 1-9). Two leucine residues (yellow) are apart from the opposite side of the lid.

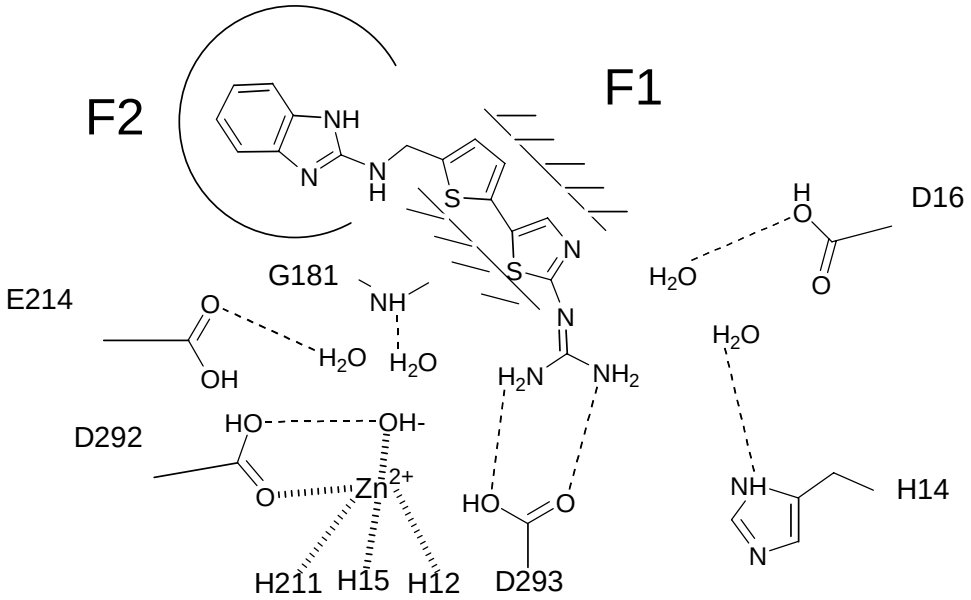

Figure1-13. Interaction mode between ADA and FR117016. The dot lines and bold dot lines show hydrogen bonds and co-ordination bonds, respectively. FR117016 interacts with ADA by two direct hydrogen bonds and a lot of hydrophobic interactions using F1 and F2 subsites. Five water molecules interact with the active site residues without the inhibitor recognition.

1-5 Conclusions

For smooth and efficient SBDD, we could achieve our goal of sufficiently rapid growth of high-quality crystals of ADA by employing crystal growth in a magnetic field.

The HDPR complexes of bovine and mouse ADA have similar conformations, and are especially identical around the active site, in spite of a mutation between the significant two leucine residues. The interaction pattern between bovine ADA and HDPR is similar to that of mouse ADA. Therefore, it can be predicted that human ADA acts in the same way as bovine and mouse ADA. This result should be useful for the structure based drug design based upon substrate analogues such as HDPR. Nevertheless, this result does not confirm that this conformation is the only stable form, or that it is one of the inhibitor-induced conformations, since HDPR can not bind to ADA without movement of the lid on the top of active site. Practically, bovine ADA could not be crystallized in the native form under the same conditions described in this paper and crystallization of mouse ADA in the native form has not been reported yet. This means that it is probably difficult to obtain the native form, and that native ADA might have a number of some different conformations in solution. Taking account of the movement as well as precise observation of the structural features, we are planing to design more effective ADA inhibitors.

According to analysis of the HDPR and FR117016 complexes, it is shown that ADA also has an open-close motion. The lid works in the incorporation of substrate and the release of reactant. Furthermore, in the middle of the motion, the lid stabilizes the reaction field. It is assumed that FR117016 also forms a stable conformation of ADA in the course of the motion.

A novel recognition site due to FR117016 binding was obtained. We believe that the structure of the FR117016 complex should provide valuable information and be of great help for drug design. We have earlier successfully produced a unique ADA inhibitor based upon the structure of the apoenzyme from the HDPR complex by means of structure-based drug design [33]. On the basis of the structural information obtained from the FR117016 complex, we plan to initiate a modification study of this compound with the aim of producing a highly potent non-nucleoside inhibitor of ADA.

1-5 References

1. Martin, D.W. & Gelfand, E.W. (1981). *Ann. Rev. Biochem*. **50**, 845-877.
2. Kameoka, J., Tanaka, T., Nojima, Y., Schlossman, S.F. & Morimoto, C. (1993). *Science* **261,** 466-469.
3. Levy, Y., Hershfield, M.S., Fernandez-Mejia, C., Polmar, S.H., Scudiery, D., Berger, M. & Sorensen, R.U. (1988). *J. Pediatr*. **113**, 213-317.
4. Marshall, E. (1995). *Science* **267**, 1588.
5. Glazer, R. (1980) in *Reviews on Drug Metabolism and Drug Interactions* **Vol.3**, 105-128, Freund Publishing House, Ltd., London.
6. Centelles, J. J., Franco, R., & Bozal, J. (1988), *J. Neurosci. Res.* **19**, 258-267.
7. Wilson, D.K., Rudolph, F.B. & Quiocho, F.A. (1991). *Science* **252**, 1278-1284.
8. Sharff, A.J., Wilson, D.K., Chang, Z. & Quiocho, F.A. (1992). *J. Mol. Biol*. **226**, 917-921.
9. Wilson, D.K. & Quiocho, F.A. (1993). *Biochemistry* **32**, 1689-1694.
10. Siederaki, V., Mohamedali, K.A., Wilson, D.K., Chang, Z., Kellems, R.E., Quiocho, F.A. & Rudolph, F.B. (1996). *Biochemistry* **35**, 7862-7872.
11. Siederaki, V., Wilson, D.K., Kurz, L.C., Quiocho, F.A. & Rudolph, F.B. (1996). *Biochemistry* **35**, 15019-15028.
12. Hershfield, M.S., Buckley, R.H., Greenberg, M.L., Molten, R., Schiff, R., Hatem, C., Kurtzberg, J., Markert, M.L., Kobayashi, A.L. & Abuchowski, A. (1987). *New. Engl. J. Med*. **316**, 589-596.
13. Wiginton, D.A., Adrian, G.S. & Hutton, J.J. (1984). *Nucleic Acids Res*. **12**, 2439-2446.
14. Kelly, M.A., Vestling, M.M., Murphy, C.M., Hua, S., Sumpter, T. & Fenselau, C. (1996). *J. Pharm. Biomed. Anal*. **14**, 1513-1519.
15. Yeung, C.Y., Ingolia, D.E., Rot, D.B., Shoemaker, C., Al-Ubaidi, M.R., Yen, J.Y., Ching, C., Bobonis, C., Kaufman, R.J. and Kellems, R.E. (1985). *J. Biol. Chem*. **260**, 10299-10307.
16. Harrison, D.H.T., Bohren, K.M., Petsko, G.A., Ringe, D. & Gabbay, K.H. (1997), *Biochemistry* **36**, 16134-16140.
17. Mande, S.C., Mainfroid, V., Kalk, K.H., Goraj, K., Martial, J.A., & Hol, W.G.J. (1994). *Protein Science* **3**, 810-821.
18. Wilson, D.K., Rudolph, F. B., Harrison, M. L., Kellems, R. E., & Quiocho, F. A. (1988). *J. Mol. Biol.* **200**, 613-614.

19. Jancarik, J. & Kim, S-H. (1991). *J. Appl. Cryst.* **24**, 409-411
20. Lin, S.-X., Zhou, M., Azzi, A., Xu, G.-J., Wakayama, N.I. & Ataka, M. (2000) *Biochem. Biophys. Res. Commun.* **275**, 275-278.
21. Cudney, B., Patel, S. and McPherson, A. (1994) *Acta Cryst.* **D50**, 479-483.
22. Garcia-Ruiz, J.M. and Moreno, A. (1994) *Acta Cryst.* **D50**, 484-490.
23. Zhu, D.-W., Lorber, B., Sauter, C., Ng, J.D., Benas, P., Grimellec, C. & Giege, R. (2001) *Acta Cryst.* **D57**, 552-558.
24. Borgstahl, G.E.O., Vahedi-Faridi, A., Lovelace, J., Bellamy, H.D. & Snell, E.H. (2001) *Acta Cryst.* **D57**, 1204-1207.
25. Pakhomova, S., Luz, J.G., Kobayashi, M., Mellman, D., Buck, J. & Newcomer, M.E. (2000) *Acta Cryst.* **D56**, 1641-1643.
26. Yin, D., Inatomi, Y. & Kuribayashi, K. (2001). *J. Cryst. Growth* **226**. 534-542.
27. Navaza, J. (1994), *Acta Cryst.* **D50**, 157-163.
28. Mande, S.C., Mainfroid, V., Kalk, K.H., Goraj, K., Martial, J.A. and Hol, W.G. J. (1994). Protein Science 3, 810-821.
29. Wilson, D.K., Tarle, I., Peterash, J.M. and Quiocho, F.A. (1993). Proc. Natl. Sci. USA 90, 9857-9851.
30. Harrison, D.H., Bohren, K.M., Ringe, D., Petsko, G.A. and Gabbay, K. (1994). *Biochemistry* **33**, 2011-2020.
31. Harrison, D.H.T., Bohren, K.M., Petsko, G.A. and Gabbay, K.H. (1997). *Biochemistry* **36**, 16134-16140.
32. Calderone, V., Chevrier, B., van Zandt, M., Lamour, V., Howard, E., Poterszman, A., Barth, P., Mitschler, A., Lu, J., Dvornik, D.M., Klebe, G., Kraemer, O., Moorman, A.R., Moras, D. and Podjarny, A. (2000). *Acta Cryst.* **D56**, 536-540.
33. Terasaka, T., Nakamura, K., Eikyu, Y., Kinoshita, T., Sato, A., Kuno, M., Seki, N. and Nakanishi, I. in press.

2. Aldose Reductase

2-1 Introduction

Aldose reductase (AR; EC 1.1.1.21) is an NADPH-dependent enzyme that catalyses the reduction of the aldehyde form of compounds to the corresponding alcohols. The enzyme belongs to the family of oxidoreductases that use NADPH as a cofactor and possesses a broad specificity for various aldo-keto compounds (figure 2-1). Although its role in the cell is not defined clearly, it is known to catalyze an important step of the polyol pathway of glucose metabolism.

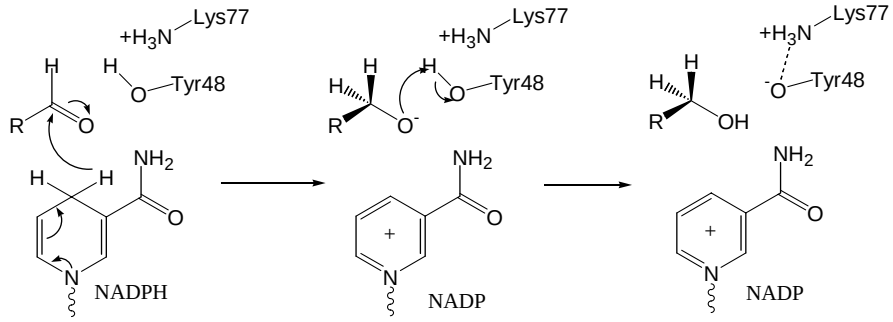

Figure 2-1. AR converts aldehyde form of compound to the corresponding allohols. First, a hydrogen atom of coenzyme NADPH attacks the carbonyl group of the aldehyde. The reactant acquires a hydrogen atom from the hydroxyl group of Tyr48. Finally, the alcohol is generated.

Clinical interest in AR has resulted from its role in reducing glucose to sorbitol. Enhanced flux of glucose through the polyol pathway is believed to be related to a number of diabetic complications, including neuropathy, nephropathy, cataracts and retinopathy. A large number of inhibitors have been, and continue to be, developed and some have shown promise in the treatment of diabetic complications. The main structural features of these inhibitors are a polar head group and a hydrophobic ring system [1]. As shown by crystal structures, whilst the hydrophobic moiety interacts with the hydrophobic cleft of the active site, the polar head group interacts with protein residues that are essential for catalysis.

As one of the promising inhibitors of this enzyme, zenarestat (figure 2-2, 3-(4-bromo-2-fluorobenzoyl)-7-chrolo-3,4-dihydro-2,4-dioxo-1(2H)-quinazolineacetic acid, has been reported to inhibit cataract formation and to counteract reduced motor nerve conduction velocity in streptozotocin-induced diabetic rats [2]. Recently, it has been demonstrated that zenarestat improved both nerve conduction velocity and nerve morphological changes in patients with diabetic peripheral polyneuropathy [3]. Zenarestat displays an IC50 of 44 nM for AR and also exhibits excellent pharmacokinetic properties in humans and is currently in Phase III clinical studies [4].

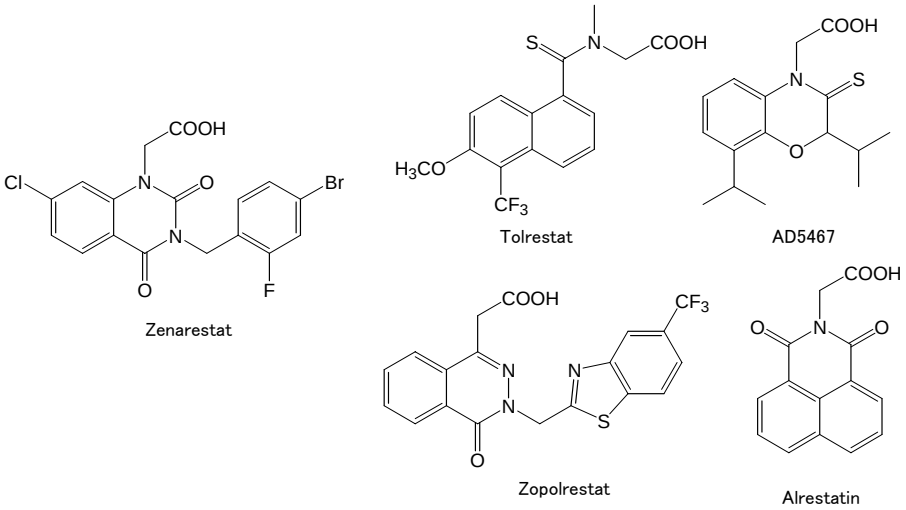

Figure 2-2. Chemical structures of potent drugs for the diabetic complications. All drugs have carbonic acid groups. This part interacts with NADPH and Tyr48, which are essential for the enzyme reaction. On the other hand, hydrophobic parts of all drugs are various. The variety results in a broad specificity for various aldo-keto compounds.

A number of quite different conformations of human AR have already been reported [5-8]. Of particular note, the hydrophobic cleft of the active site has high flexibility to correspond to the broad specificity for substrates and inhibitors. This flexibility results in dramatic movements and each conformation can form one of three different crystal forms: triclinic, monoclinic and orthorhombic. Since zenarestat belongs to a novel structural class of AR inhibitors, we could not predict *a prior* the crystal form or the binding mode in detail. Careful observation of the structure of a complex of AR and zenarestat is essential to understanding the mode of action of this class of inhibitors and for rational design of better therapeutics. Herein, we report the structure of AR complexed with zenarestat.

2-2 Materials and Methods

2-2-1 Crystallization

Human recombinant AR was purchased from Wako Pure Chemical Industries Ltd., and zenarestat was prepared at our company. The protein solution was used with no further purification for the crystallization, and was employed at 14 mg/ml in 50 mM citrate buffer at pH 5.0 and 7 mM 2-mercaptoethanol with 1 mM zenarestat suspended. All crystallization trials were carried out by the hanging drop method of vapor diffusion

by mixing 2 μl of the protein solution with 2 μl of the reservoir solution and equilibrating the drops over the reservoir at room temperature.

All of the published reports show that AR crystallized using the same precipitant at the same pH: polyethyleneglycol 6000 at pH 5.0, although those crystals classified into three crystal forms. Therefore, the first trial was done using grid sceening referred to the conditions for the crystallization in these reports: 15 - 25 % (w/v) polyethylene glycol 6000, 50mM citrate buffer at pH 5.0. Finally, the crystals of human AR complexed with zenarestat used for data collection were grown against reservoirs containing 20 - 22.5 % (w/v) polyethylene glycol 6000 in 50 mM citrate buffer at pH 5.0. The crystals grew to maximum dimensions of approximately 0.15 x 0.10 x 0.05 mm in 2 weeks.

2-2-2 Data collection and refinement

After dipping in a solution of paratone-N (Hampton Research Inc.), the X-ray diffraction data were collected at 100 K using synchrotron facilities [9] at beam line BL6B of Photon Factory, Japan for Structural Biology Sakabe Project. The crystal-to-imaging-plate distance was 573 mm and the oscillation range was 7 degrees. The image data were processed using DENZO [10] and SCALEPACK [11] (table 2-1).

The structure of human AR complexed with zenarestat was solved by the molecular replacement method using the program AMoRe [12] in the CCP4 suite. This complex crystallized in the triclinic form with similar cell constants to that registered as 1MAR [7] in the Protein Data Bank (PDB). However, because only the atomic coordinates of the Cα atoms were available for 1MAR, the holoenzyme of the orthorhombic form (1ADS in PDB) was used as a search model for structure solution. After a rigid-body refinement, the zenarestat molecule was placed in the electron density by a Fourier difference map. The model of the complex was used as the starting point of the refinement, which included a rigid- body refinement step, slow cooling step, Powell minimization and a temperature factor refinement. Water molecules were then placed in a difference map (2 σ level) and minimization was performed. The program X-POLR [13], Quanta (Molecular Simulations, Inc.) and X-solvate (Molecular Simulations, Inc.) were used for refinement, model building and picking of water molecules, respectively.

Table 2-1. Data collection and refinement statistics of the complex of human recombinant AR and zenarestat**.**

Data collection and processing	
Unit cell parameters	
a, b, c (Å)	40.37, 47.69, 47.94
α, β, γ (°)	76.0, 67.5, 76.7
Diffraction data	
dmin (Å)	2.5
Unique reflections	10335
Rsym (%)	6.0 (9.1)
Completeness (%)	94.6 (83.7)
Redundancy	2.2 (2.1)
I/σ(I)	17.7 (16.7)
Rigid body refinement	
Resolution (Å)	8.0-4.0
Rcryst (%)	27.4
Refinement	
Resolution (Å)	8.0-2.5
Reflections used[*F > 2s(F)*]	9831
Rcryst/Rfree (%)	17.8/19.9 (19.7/22.7)
Final model	
Protein residues	316
Coenzyme	1
Inhibitor	1
Water	186
R.M.S. diviations	
Bonds (Å)	0.039
Angles (Å)	4.4
Dihedrals (Å)	29.8

Values in parentheses are for the highest shells (2.59-2.50 Å).

2-3 Structure of Zenarestat complex

As mentioned above, this complex crystallized in triclinic form with similar cell constants to the complex with the inhibitor, zopolestat (1MAR in PDB). Thus, the Cα backbone structures of holoenzyme in the two complexes are very similar to each other with an RMSD value of 0.59 Å (figure 2-3), although the two dimensional formulas of these inhibitors are different. Both inhibitors occupied almost the same site in the respective complexes. However, the detailed structures of these complexes, such as inhibitor-induced conformational change of the side chains, are quite different. Therefore, careful and precise observation of the active site is required to provide hints for effective modification of this class of inhibitors.

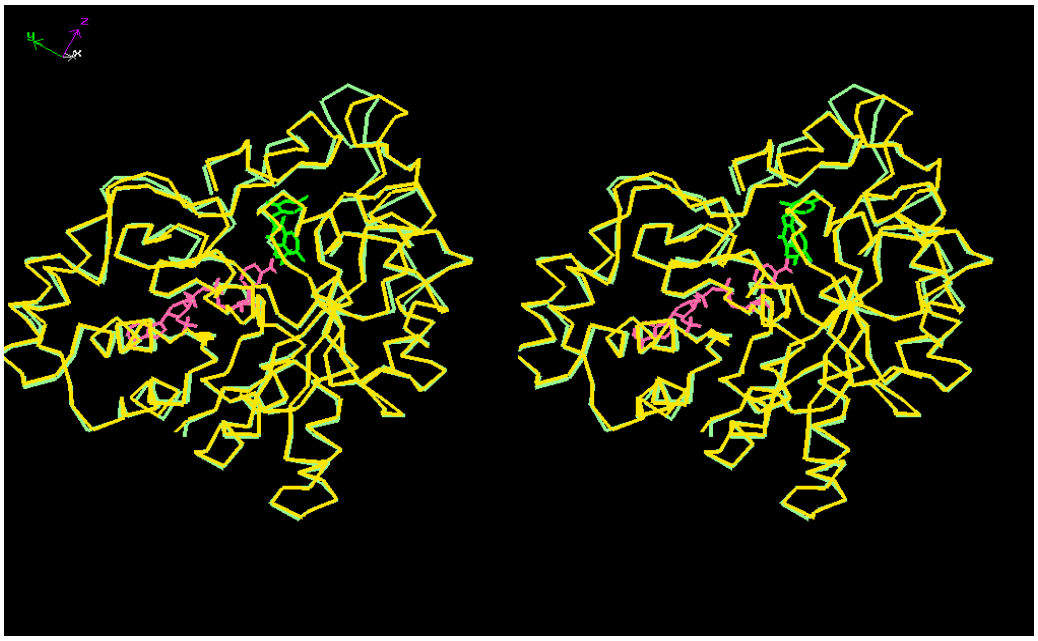

Figure 2-3. A stereo view of superimposed α-carbon backbone structures of the complex with zenarestat (holoenzyme: yellow, NADPH: pink, zenarestat: green) and of the holoenzyme registered as 1MAR at Protein Data Bank (white). The two holoenzyme molecules have almost the same backbones, except for the loop on the upper right of the active site.

Bound zenarestat, with its unambiguous difference electron density map (figure 2-4a), occupies almost the whole active site cleft at the top of the β barrel (figure 2-3). The bound inhibitor is almost buried in the active site cavity; it has an accessible surface area of 46.8 $Å^2$, 8.0 % of the total surface area of the unbound inhibitor. The binding mode indicated many features consistent with its potent inhibition. The quinazoline ring is almost at a right angle to and bisects the plane of the benzene ring, protruding from the center of the pocket. It is also perpendicular to the nicotinamide ring of NADPH.

There is excellent complementarity between bound zenarestat and the active site of

AR. The inhibitor makes an unusually large number of contacts with the active site, totaling 110 contacts within a 4 Å distance - 92 with 13 residues, 15 with the nicotinamide moiety of NADPH, and 3 with 3 ordered water molecules. The hydrophilic head makes a network of hydrogen bonds to the catalytic site (figure 2-4b). That is, one acid oxygen forms three hydrogen bonds with Nε2 of His110 (2.6Å), Oη of Tyr48 (2.9Å), and the carbonyl oxygen of NADPH (2.6Å). The other oxygen forms a hydrogen bond with Nε1 of Trp111 (2.9Å). The two carbonyl oxygen atoms of the quinazoline ring make hydrogen bonds with a side chain of AR and a water molecule, respectively. The 2-carbonyl oxygen of the ring forms a hydrogen bond with Sγ of Cys298 (3.5Å), and the 4-carbonyl oxygen with water127 (2.8Å). The hydrophobic moiety, including the two ring systems of the inhibitor, binds to the hydrophobic active site consisting of 11 amino acids; Trp20, Val47, Trp79, His110, Trp111, Thr113, Phe121, Phe122, Tyr219, Ala299, and Leu300. The benzene ring of zenarestat cuts in to the side chains of Leu300 and Trp111 that interact directly and form a CH-π interaction in the native holoenzyme (figure 2-5a). As a result, these two side chains and zenarestat form a quite unique CH-π-π interaction (figure 2-5b). The benzene ring hereby forms a π-π interaction to the indole ring of Trp111 and a CH-π interaction to the methyl group of Leu300. The other induced fitting is found at the amino acids near the Br atom of bound zenarestat, where the side chains were found to be moved significantly (Tyr309 OH: 4.7Å, Phe115 Cζ: 4.3Å). Consequently, the Br atom forms a hydrogen bond to the OH group of Tyr309: 3.4Å. These inhibitor-induced conformational changes indicate why the selectivity of the hydrophobic site is very broad.

2-4 Conclusion

Through the crystal structures solved so far including this complex, the portion binding the polar head group of the inhibitor is structurally stable. Therefore, considering this portion of these inhibitors as a rigid template, the polar head part may be readily modified. The high flexibility of the hydrophobic part, however, makes it difficult to design the hydrophobic part of an inhibitor. We believe that the structural information reported herein should be helpful for major improvement of several properties of this class of inhibitors essential to succeed as a medicine, for example, solubility in water, toxicity, and metabolism. However, it is noted that if major structural modification is examined, it is recommended to certify the enzyme-inhibitor interaction by X-ray analysis.

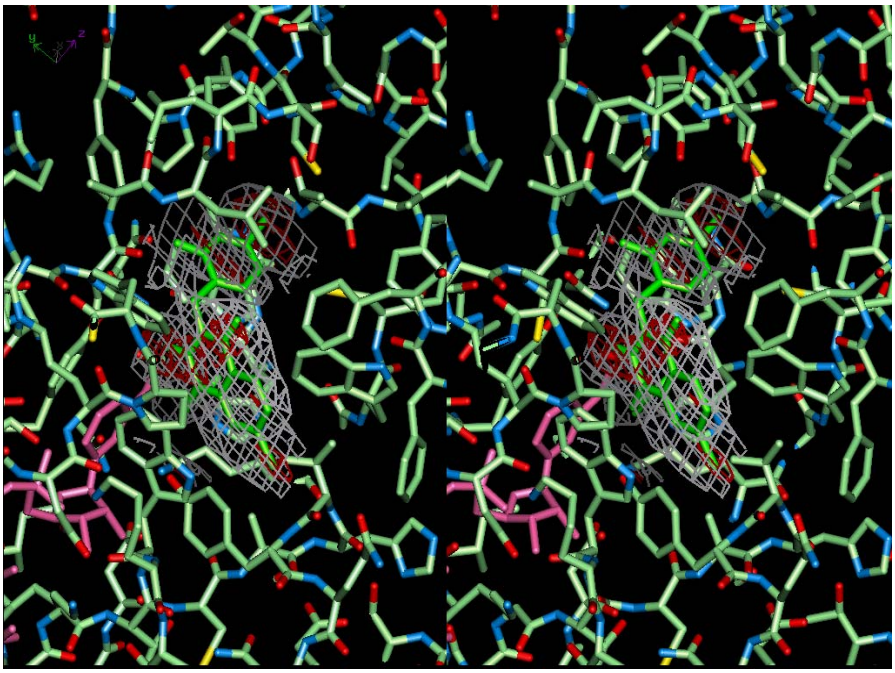

(a)

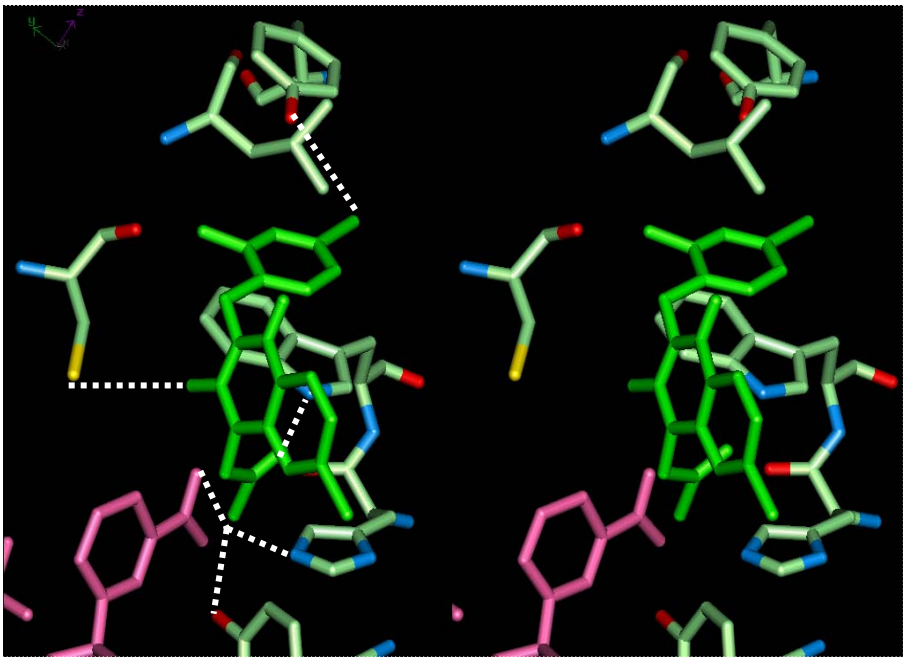

(b)

Figure 2-4. Stereo views of the active site (zenarestat: green, NADPH: pink, oxygen atoms: red, nitrogen atoms: blue, sulfur atoms: yellow, carbon atoms: white). (a) The inhibitor is enclosed in a wire-cage representation of the electron density map calculated at 2.5 Å resolution by a Fourier transform using $|Fo| - |Fc|$ as coefficients (grey line: 1 σ level map, red line: 3 σ level map). Fc values calculated from the initial protein structure. The electron density at heavy atom positions (Br, Cl) and two carbonyl groups of the quinazoline ring is higher than that of the other atoms of the inhibitor. (b) Zenarestat makes six hydrogen bonds with AR. The hydrogen bonds are displayed as the white dot lines.

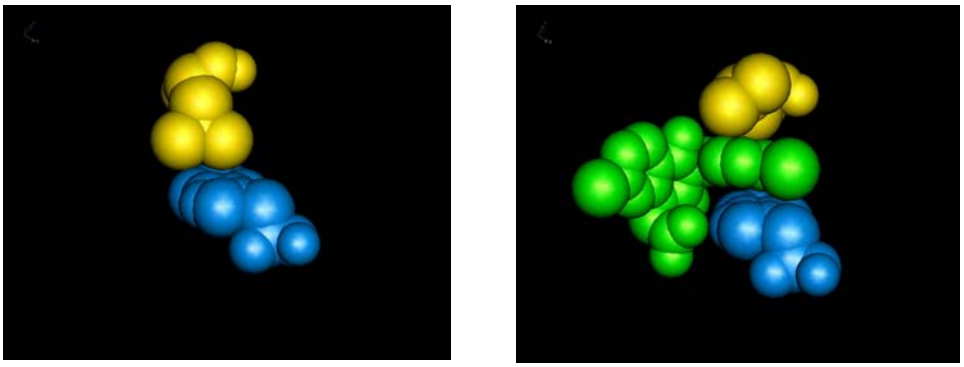

Figure 2-5. Space-filled models. (a) The side chains of Leu300 (yellow) and Trp111 (blue) make a CH-π interaction in the native holoenzyme. (b) The benzene ring of zenarestat (green) and the two upper side chains form a CH-π-π interaction in this complex.

2-5 References

1. Lee, Y.S., Pearlstein, R., & Kador, P.F. (1994), *J. Med. Chem.* **37**, 787-792.
2. Ao, S., Kikuchi, C., Ono, T., & Notsu, Y. (1991), *Investigative Ophthalmology & Visual Science* **32**, 3078-3083.
3. Greene, D.A., Arezzo, J.C. & Brown, M.B. (1999), *Neurology* **53**, 580-591.
4. Takakura, S., Minoura, H., Shimoshige, Y., Minoura, K., Kawamura, I., Fujiwara, T., Saitoh, T., Shimojo, F., Seki, J., & Goto, T., in press (*Drug Development Research)*
5. Calderone, V., Chevrier, M. van Z., Lamour, V., Howard, E., Poterszman, A., Barth, P., Mitschler, A., Lu, J., Dvornik, D.M., Klebe, G., Kraemer, O., Moorman, A.R., Moras, D. & Podjarny, A. (2000), *Acta Cryst.* **D56**, 536-540.
6. Harrison, D.H.T., Bohren, K.M., Petsko, G.A., Ringe, D. & Gabbay, K.H. (1997), *Biochemistry* **36**, 16134-16140.
7. Wilson, D.K., Bohren, K.M., Gabbay, K.H. & Quiocho, F.A. (1992), *Science* **257**, 81-84.
8. Wilson, D.K., Tarle, I., Peterash, J.M. & Quiocho, F.A. (1993), *Proc. Natl. Acad.Sci. USA* **90**, 9847-9851.
9. Sakabe, N. (1991), *Nucl. Instrum. Methods A* **303**, 448-463.
10. Otwinoski, Z. (1997), *Methods Enzymol.* **276**, 307-326.
11. Fox, G.C. & Holmes, K.C. (1966), *Acta Cryst.* **20**, 886-891.
12. Navaza, J. (1993), *Acta Cryst.* **D49**, 588-591.
13. Brunger, A.T. (1992), *X-PLOR version 3.1: A System for X-ray Crystallography and NMR*. Yale University Press, New Haven, CT., USA.

3. Elastase

3-1 Introduction

Elastase is a serine protease classified in the chymotrypsin family, and is possibly the most destructive enzymes having the ability to degrade virtually all of the connective components in the body. Reaction mechanism of serine protease and definition of the nomenclatures for enzyme study are shown in figure 3-1 and figure 3-2, respectively. Uncontrolled proteolytic degradation by elastase has been implicated in a number of pathological conditions. Pancreatic elastase (EC 3.4.21.36) causes the fatal disease pancreatitis, and leukocyte elastase (EC 3.4.21.37) has been implicated in a number of inflammatory disorders. Highly selective drugs for each elastase can suppress the side effects due to other elastases [1].

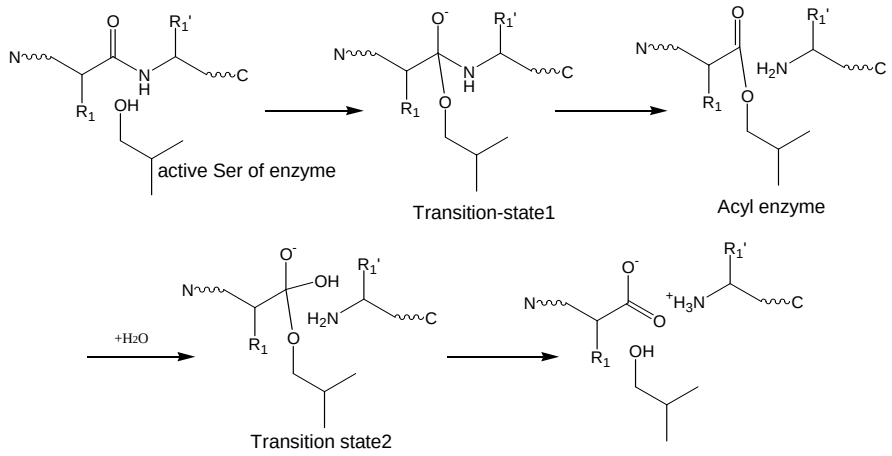

Figure3-1. Reaction mechanism of serine protease. First, activated Ser188 Oγ attacks a peptide bond of substrate and forms the transition-state1. By a base (histidine) attacking, C terminal portion leaves from the state1 and N terminal portion forms acyl enzyme. After addition of a water to acyl-enzyme, via the transition state2, N terminal portion also leaves from enzyme.

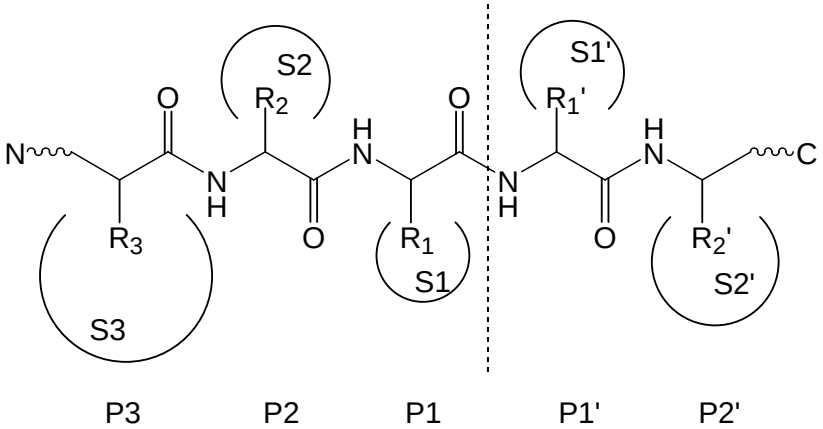

Figure3-2. Definitions of the nomenclatures for peptide residues of substrate (or inhibitor) and for subsites of enzyme active site. Substrate cleavages at the peptide bond shown as dashed line. For example, Side chain R1 of residue P1 fits into the subsite S1. Significant subsite is differing from each enzyme. Elastase recognizes the substrate mainly using subsite S1.

Structural studies have been described using two elastases: human leukocyte elastase (HLE) consisting of 218 amino acids and porcine pancreatic elastase (PPE) consisting of 240 amino acids. Although the amino acid sequence homology of the two elastases is only 37 %, the backbone architecture of both elastases is conserved, and the structures of the active sites near the cleavage site are very similar. The S1 pocket recognizes small hydrophobic groups such as alanine, valine or leucine. The S2 and S3 pockets are wide and broad hydrophobic areas. On the other hand, the S4 and S5 pockets, which are remote from the cleavage site, are quite different. Careful observation of this difference may lead to compatible structure based drug design (SBDD) and may allow design of selective inhibitors for the respective elastases. Nevertheless, a large number of non-selective inhibitors have been researched and developed by SBDD.

FR136706,2-[4-[[(S)-1-[[(S)-2-[[(RS)-3,3,3-trifluoro-1-isopropyl-2-oxopropyl] aminocarbonyl]pyrrolidin-1-yl-]carbonyl]-2-methylpropyl]aminocarbonyl] benzoylamino]acetic acid (figure 3-3a), is an example of a potent peptidyl inhibitor with no selectivity for the two elastases. FR136706 is structurally similar to MDL101146 (Figure 3-3b), and structures of HLE and PPE complexed with MDL101146 have been already reported [2]. Based upon those structures, the binding modes of FR136706 can be easily predicted because of the similarity in their chemical structures. Thus, the terminal valine residue is deduced to bind at the S1 pocket. The P1 to P4 residues of FR136706 can then be assigned corresponding to the S1 to S4 pockets of the enzyme. However, the terminal glycine moiety can not be confirmed as a P5 residue from the assumed binding model.

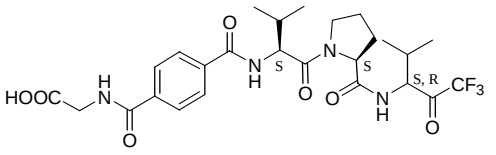

P4 P3 P2 P1

(a) FR136706

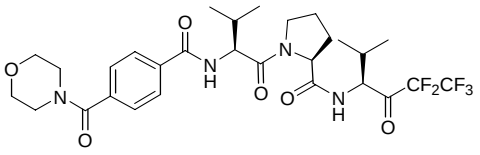

P4 P3 P2 P1

(b) MDL101146

Figure3-3. Chemical structures of elastase inhibitors. (a) Structure of FR136706. This compound is suggested to have P1-P4 residues from a model of the complex. The terminal glycine moiety can not be assigned. (b) Structure of MDL101146. P1-P4 residues assigned based upon the structure of the complex.

Selectivity for the two elastases may be easily achieved if the real interaction modes of an inhibitor are available for both enzymes. The precise and complete structure of the FR136706-HLE complex can be easily modeled based upon the MDL101146-HLE complex. On the other hand, the binding mode of the FR136706-PPE complex is difficult to predict due to the following reasons. First, the morpholino moiety of MDL101146 in the PPE complex is exposed to the solvent region. Second, the Arg217 side chain is unnaturally fastened by an adjacent elastase molecule in the MDL101146-PPE complex crystal. Arg217 is essential for the recognizing P4 residue [3] and for biological activity. The chemical modification of Arg217 leads to an 85 % loss of activity toward the specific substrate N-succinyltrialanine p-nitroanilide [4]. The crystal packing of the MDL101146 complex is mainly responsible for the structural unreliability around Arg217. The crystal of the complex belongs to the trigonal form with space group *R*3, which is different from the orthorhombic form of the native and many other complexes. This packing ensures that MDL101146 complex molecules can not make the same interaction network as in the orthorhombic crystals.

In order to succeed in the selective SBDD, it is necessary to investigate the true and precise interaction mode including the side chain of Arg217. Here we determine the structure of FR136706-PPE complex with natural interactions. Subsequently, careful observation and comparison of these regions in both elastases may lead to successful SBDD.

3-2 Materials and Methods

3-2-1 Crystallization

Commercially available PPE was purchased from Worthington Biochemicals and used without further purification. FR136706 was produced at our company. The complex solution was prepared by directly dissolving the inhibitor at a final concentration of 1 mM into the protein solution. Crystals of the complex were prepared under the similar crystallization conditions of native PPE [5].

3-2-2 Data collection and structure determination

X-ray data for the complex were collected at room temperature on a Rigaku R-AXIS-IIc. Graphite monochromatized MoKα radiation (λ=0.7107 Å) was produced by a Rigaku RU-200 X-ray generator operated at 50kV and 90mA. The oscillation images were indexed and integrated by the program PROCESS [6] (table 3-1).

The difference Fourier map was calculated using the phases and amplitude obtained from the native structure [7] (PDB code: 3EST) without ions and solvent molecules. Active serine Oγ was in an envelope of the density continuous with the inhibitor and likewise covalently attached. A model with the *S* configuration at Cα of the P1 valine residue could easily fit onto the difference map.

After fitting the inhibitor onto the difference Fourier maps, the areas of ions existing in the native structure were checked. A sulphate ion and a calcium ion were conserved in the native structure, and these ions were assigned at the envelope center with the highest density of the map. The model of the complex was used as the starting point of refinement, which included a rigid-body refinement step, slow cooling step, Powell minimization step and a temperature factor refinement. Water molecules were then picked up in a difference map at the 3 σ level and minimization was performed. The programs X-PLOR [8], Quanta (Accelrys) and X-solvate (Accelrys) were used for refinements, model building and picking water molecules, respectively. Coordinate data have been deposited in the Protein Data Bank under the code 1MMJ.

Table 3-1. Data collection and refinement statistics of FR136706 complexed with porcine pancreatic elastase

Data collection and Processing	
Space group	$P2_12_12_1$
Unit cell parameters (Å)	a=51.29, .52, b=58.31, c=75.52
Resolution (Å)	2.20
R_{sym} (%)	8.2(15.1)
Completeness (%)	94.6(90.9)
Redundancy	3.1(1.5)
I/σ(I)	9.6(4.4)
Refinement	
R_{cryst} (%)	21.5(22.7)
R_{free} (%)	24.1(26.2)

Values in parentheses are for the highest shell (2.35-2.20 Å).

3-3 Structure of FR136706 complex

Crystals of FR136706 complexed with PPE grew in 1-2 months and had typical dimensions of 0.4 X 0.15 X 0.15 mm. These crystals belonged to the orthorhombic form, which is the same as those of the other many complexes. Within a 5 Å distance around the side chain of Arg217, no other PPE molecules except for water molecules were present. The side chain of Arg217 therefore has no conformational change due to alignment in the crystal. Therefore, the conformation in this crystal should reflect the *in vivo* situation.

The Cα backbone structures of holoenzyme in the native and FR136706 complex form are very similar to each other, with a r.m.s.d value of 0.31 Å. The Cα backbone structures of holoenzyme in the native and MDL101146 complex are also similar with a r.m.s.d value of 0.48 Å. Concerning backbone atoms, the structure of PPE itself is very rigid and unchanged when inhibitors bind to PPE, although some enzymes, such as aldose reductase, are known to have big movement in backbone structure through inhibitor-inducing [9]. Therefore, careful and precise observation of the slight but critical movement of side chains can directly lead to successful SBDD.

Near the cleavage site, FR136706 fits snugly in the extended active site pocket with a similar interaction mode to the other inhibitors [10,11]. FR136706 makes a total of seven hydrogen bonds, a covalent bond and many hydrophobic interactions with the

PPE molecule (figure 3-4). The oxy-anion hole, which plays a key role in the recognition and stabilization of the carbonyl group of a substrate, is occupied by a hydroxyl group, which forms hydrogen bonds with Gly186 NH and active Ser188 NH (2.72 Å and 2.65 Å). FR136706 also forms an antiparallel sheet structure with Ser207 and Val209 by three hydrogen bonds: P1 NH to Ser207 CO: 3.08 Å; P3 CO to Val209 NH: 2.86 Å; P3 NH to Val209 CO: 2.71 Å. A fluorine atom and His45 Nε make a hydrogen bond with a distance of 2.66 Å. Hydrophobically, the P1, P2 and P3 side chains interact with the corresponding S1-S3 pockets. The terminal glycine turns to the solvent region, and the carbonyl group forms hydrogen bonds with two water molecules as well as with the side chains of Arg21 and Ser52 in the symmetry-related PPE molecule. The carbonyl group of the P4 residue also makes a hydrogen bond with Th 167 Oγ (2.86 Å).

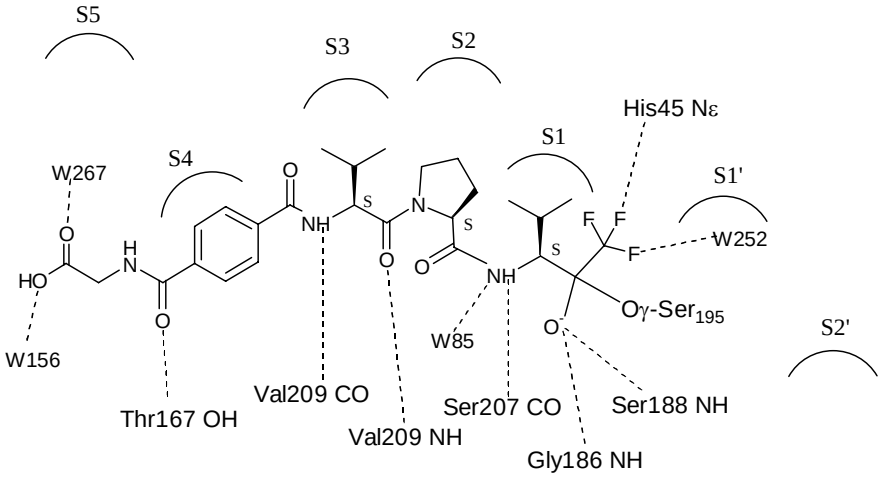

Figure 3-4. Interaction of FR136706 complex. FR136706 binds to PPE by seven hydrogen bonds, a covalent bond and many hydrophobic interactions. Dotted lines show hydrogen bonds in the complex.

The side chain moiety of the noteworthy Arg217 residue locates on the benzene moiety of FR136706 and both moieties form a π-π interaction (figure 3-6). The average distance between the benzene atoms of the inhibitor and the guanidyl atoms of Arg217 is 3.5 Å. In the MDL101146 complex, Arg217 does not cap the benzene moiety at all (figure 3-5). Arg217 in the native structure is apart from the protein surface and exposed to the solvent region. Therefore, the conformation of Arg217 is suggested to be induced by FR136706 binding and to be important for inhibitor recognition. As a result of Arg217 movement, the S3 pocket becomes clearer, and is extended along with the ethylene chain of Arg217. In the native structure, the S3 pocket is broad and seems to be unimportant for inhibitor recognition. Furthermore, Arg217 movement results in emergence of a clear S5 pocket, although the side chain of Arg217 partially occupies the pocket in the MDL101146 complex.

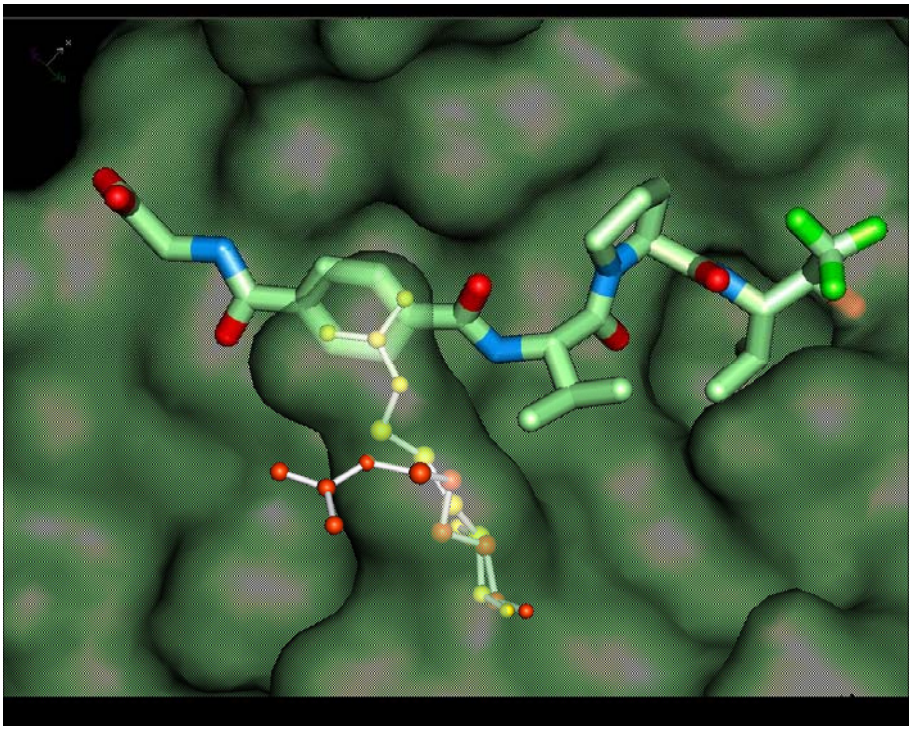

Figure 3-5. FR136706 (stick model) on the surface of PPE. The two side chains of Arg217 in the FR136706 and MDL101146 complexes are shown as yellow and red ball-and-stick models, respectively. The side chain moiety of Arg217 greatly moves and caps the benzene moiety of FR136706. Both moieties form a π-π interaction**.**

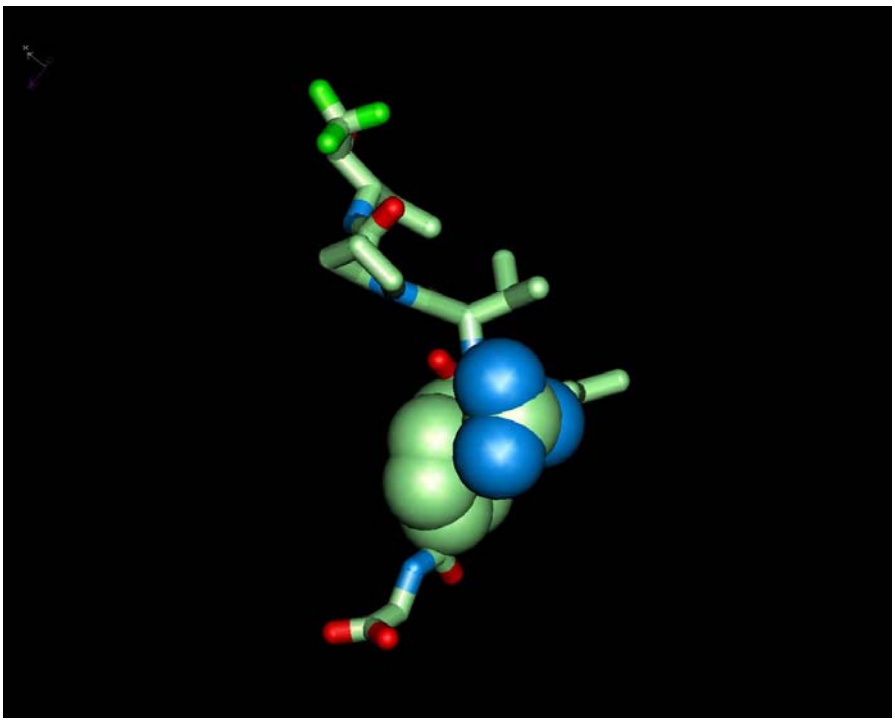

Figure 3-6. An interaction between the benzene moiety of FR136706 and the guanidyl moiety of Arg217. Both moieties forming a π-π interaction are shown by space-filled sphere model. The other part of FR136706 is shown as stick model.

3-4 Conclusion

A novel interaction mode in an FR136706-PPE complex involving unique Arg217 movement has been discovered. Based upon this structure, we believe the activity of FR136706 can be improved effectively. Initially, PPE selective design is considered, since HLE selective design can be applied more effectively if PPE structures are available and are understood precisely.

The P1 valine residue exactly fits the S1 pocket, suggesting that the P1 residue is critical. The S2 pocket has an extra hydrophobic and broad area extended in the directions to the Cβ and Cγ atom of the P2 proline residue. Practically, several modifications toward this space to obtain effective inhibitors have already been reported [12].

The P3 valine residue can be replaced with bigger groups such as leucine or isoleucine, since Arg217 movement causes extension of the S3 pocket. In the native or other complexes, the S3 pocket is broad or ambiguous because Arg217 is in the solvent region. Therefore, it has been difficult to come up with effective design for the S3 pocket.

The P4 benzene moiety sits down on the hydrophobic surface consisting of the side chains of Phe208, Val88 and Ala89, and is capped by the Arg217 side chain. The benzene moiety sandwiched by the side chains of PPE is essential for inhibitor binding. A water molecule, forming a hydrogen bond with Asp86, is also present 4.8 Å from the same plane of the benzene moiety. As an application of a method for mimicking the structural water molecule [13], the water molecule can be introduced to the benzene moiety with two or three spacer atoms.

The terminal glycine residue is exposed to the solvent region and interacts with an adjacent PPE molecule. Therefore, the glycine can not be assigned as a P5 residue at all, and does not participate in the interaction, although it does play an important role to increase the solubility of FR136706 itself. In fact, the inhibitor with the glycine removed from FR136706 has the same activity for elastases. On the other hand, the S5 pocket, newly emerged by Arg217 movement, is empty and a hydrophobic group can be introduced to this pocket, consisting of Trp164 and ethylene chain of Lys219.

Based upon the structural information from this experiment, FR136706 derivatives with selectivity for PPE may be produced. Furthermore, compatible SBDD using the structures of both complexes with PPE and HLE may lead to selective and effective inhibitors. Careful observation of the structural differences of the S3, S4 and S5 pockets in both elastases should lead to success.

3-5 References

1. Clemente, A.; Domingos, A.; Grancho, P.; Iley, J.; Moreira, R.; Neres, J.; Palma, N.; Santana, A. B.; Valente, E. *Bioorg. Med. Chem. Lett.* **2001**, *11*, 1065-1068.
2. Cregge, R. J.; Durham, S. L.; Farr, R. A.; Gallion, S. L.; Hare, C. M.; Hoffman, R. V.; Janusz, M. J.; Kim, H.-O.; Koehl, J. R.; Mehdi, S.; Metz, W. A.; Peet, N. P.; Pelton, J. T.; Schreuder, H. A.; Sunder, S.; Tardif, C. *J. Med. Chem.* **1988**, *41*, 2461-2480.
3. Nakanishi, I.; Kinoshita, T.; Sato, A.; Tada, T. Biopolymers **2000**, *53*, 434-445.
4. Davril, M.; Jung, M. L.; Duportail, G.; Lohez, M.; Han, K. K.; Bieth, G. J. *J Biol. Chem.* **1984**, *259*, 3851-3857.
5. Sawyer, L.; Shotton, D. M.; Campbell, J. W.; Wendell, P. L.; Muirhead, H.; Watson, H. C. *J. Mol. Biol.* **1978**, *118*, 137-208.
6. Sato, M.; Yamamoto, M.; Imada, K.; Katsube, Y.; Tanaka, N.; Higashi, T. *J. Appl. Cryst.* **1991**, *23*, 348-357.
7. Meyer, E.; Cole, G.; Radhakrishnan, R. *Acta Cryst.* **1988**, *B44*, 26-38.
8. Brunger, A. T. *X-POLR version 3.1: A System for X-ray Crystallography and NMR*. Yale University Press, **1992**.
9. Kinoshita, T.; Miyake, H.; Fujii, T.; Takakura, S.; Goto, T. *Acta Cryst.* **2002**, *D58*, 622-626
10. Takahashi, L. H.; Radhakrishnan, R.; Rosenfield, R. E.; Meyer, E. F.; Trainor, D. A. *J. Am. Chem. Soc.* **1989**, *111*, 3368-3374.
11. Mattos, C.; Giammona, D. A.; Petsko, G. A.; Ringe, D. *Biochemistry* **1995**, *34*, 3193-3203.
12. Edwards, P. D.; Andisik, D. W.; Strimpler, A. M.; Gomes, B.; Tuthill, P. A. *J. Med. Chem.* **1996**, *39*, 1112-1124.
13. Lam, P. Y. S.; Jadhav, P. K.; Eyermann, C. J.; Hodge, C. N.; Ru, Y.; Bacheler, L. T.; Meek, J. L.; Otto, M. J.; Rayner, M. M.; Wong, Y. N.; Chang, C-H.; Weber, P. C.; Jackson, D. A.; Sharpe, T. R.; Erickson-Viitanen, S. *Science* **1994**, *263*, 380-384.

Concluding remarks

In chapter 1, the results of experiments in three different environments, I optimized the conditions for crystallization of the ADA-inhibitor complexes in terms of crystal quality and harvest period simultaneously. The modification was essential for successful SBDD of ADA. HDPR was almost buried in the active site by the lid of the envelope consisting two peptide components. While, novel hydrophobic spaces in addition to the well-known active site, which had been found out in the complexes with the substrate derivatives such as HDPR, were discovered in the FR117016 complex. The thiophene moiety of FR117016 was fit into the peptide lid, and they form a CH-π-π interaction.

In chapter 2, I discovered a new conformation of AR in the zenarestat complex. Consequently, the benzene moiety of the inhibitor slides into a π-π interaction involving Leu300 and Trp111, which directly interacts in other complexes and the native form. These moieties form a novel interaction mode, namely a CH- π-π interaction.

In chapter 3, I found out a critical change in the active site induced by the sole amino acid Arg217 in the PPE-FR136706 complex. In result of this move, the side chain of Arg217 and benzene moiety of FR136706 form a π-π interaction. In addition that, the S3 and S5 subsites became to be open or spread. These spaces are useful in producing novel drugs.

I proved that the proteins have several conformations due to binding with different inhibitors. In this thesis for the three proteins, ADA, AR and PPE, unknown conformational changes were discovered. Careful observation of the new interaction mode at atomic resolution may lead to the rapid discovery of an original inhibitor rationally and effectively. Specifically, the common characteristic interaction mode, CH- π-π or π- π interaction, was found out around the portions moved by inhibitor induction. Therefore, this kind of interaction is a significant key for the SBDD considering inhibitor-induced conformational change. In respective SBDD on the movable protein such as these three protein, it is first dominant to search for the CH- π interaction which can form the CH- π-π interaction and for the unsteady residues which can form the π- π interaction such as phenylalanine, tyrosine, lysine, and arginine. Intentional formation of these interactions should lead to generate structurally original and effective drugs.

List of Publications

Papers related to this thesis

1) Crystallization and Preliminary Analysis of Bovine Adenosine Deaminase
   Takayoshi Kinoshita, Nobuya Nishio, Akihiro Sato, and Masayoshi Murata
   Acta Cryst. **D55,** 2031-2032, (1999)

2) Crystallization and Preliminary X-ray analysis of cephalosporin C acylase from Pseudomonas sp. strain N176
   Takayoshi Kinoshita, Toshiji Tada, Yoshimasa Saito, Yoshinori Ishii, Akihiro Sato, and Masayoshi Murata
   Acta Cryst. **D56**, 458-459, (2000)

3) The structure of human recombinant aldose reductase complexed with the potent inhibitor zenarestat
   Takayoshi Kinoshita, Hiroshi Miyake, Takashi Fujii, Shoji Takakura and Toshio Goto
   Acta Cryst. **D58**, 622-626, (2002)

4) Crystal structure of bovine adenosine deaminase complexed with 6-hydroxyl-1,6-dihydropurine riboside
   Takayoshi Kinoshita, Nobuya Nishio, Isao Nakanishi, Akihiro Sato and Takashi Fujii
   Acta Cryst. **D59**, 299-303, (2003)

5) Improving quality and harvest period of protein crystals for structure based drug design: effects of a gel and a magnetic field on bovine adenosine deaminase crystals
   Takayoshi Kinoshita, Mitsuo Ataka, Masaichi Warizaya, Masahiro Neya and Takashi Fujii
   Acta Cryst. in press

6) True interaction mode of porcine pancreatic elastase with FR136706, a potent peptidyl inhibitor
   Takayoshi Kinoshita, Isao Nakanishi, Akihiro Sato and Toshiji Tada
   Bioorganic & Medicinal Chemistry Letters **13**, 21-24, (2003)

7) Dramatic inhibitor-induced structural change of the active site of bovine adenosine deaminase
   Takayoshi Kinoshita, Isao Nakanishi, Nobuya Nishio, Akihiro Sato, Masako Kuno, Nobuo Seki, Tadashi Terasaka, and Takashi Fujii
   In preparation

Other papers

1) Crystallization and main-chain structure of neutral protease from *Streptomyces caespitosus*
Sigeharu Harada, Kengo Kitadokoro, Takayoshi Kinoshita, Yasushi Kai, and Nobutami Kasai
J. Biochem. **110**, 46-49, (1991)

2) Synthesis of New 1,8-Bridged Tricyclic Quinolones by a Novel Intramolecular Arylation of N-1 Tethered Malonamides
David Barrett, Hideo Thuthumi, Takayoshi Kinoshita, Masayoshi Murata, and Kazuo Sakane
Tetrahedron **51**, 11125-11140, (1995)

3) Asymmetric Synthesis of FR165914: A Novel b3-Adrenergic Agonist with a Benzocycloheptane Structure
Kouji Hattori, Masanobu Nagano, Takeshi Kato, Isao Nakanishi, Keisuke Imai, Takayoshi Kinoshita, and Kazuo Sakane
Bioorganic & Medicinal Chemistry Letters **5**, 2821-2824, (1995)

4) Complete amino acid sequence of a zinc matalloendoprotease from *Streptomyces caespitosus*
Shigeharu Harada, Takayoshi Kinoshita, Nobutami Kasai, Susumu Tsunasawa, and Fumio Sakiyama
Eur. J. Biochem. **233**, 683-686, (1995)

5) A novel [3+2] annulation: synthesis and X-ray crystallographic structure of a novel tetrahydropyrazolo[1,5-a]quinoline, an intermediate towards new tricyclic quinolone antibacterials
David Barrett, Hiroshi Sasaki, Takayoshi Kinoshita, and Kazuo Sakane
Chem. Commun., 61-62, (1996)

6) Studies on Cerebral Protective Agents. IX. Synthesis of Novel 1,2,3,4-Tetrahydroisoquinolines as N-Methyl-D-aspartate Antagonists
Mithuru Ohkubo, Athushi Kuno, Kiyotaka Kathuta, Yoshiko Ueda, Kiyoharu Shirakawa, Hajime Nakanishi, Isao Nakanishi, Takayoshi Kinoshita, and Hisashi Takasugi
Chem. Pharm. Bull. **44**, 95-102, (1996)

7) Alkylation of 1-[N-(Hydroxymethyl)-N-methylamino]-4-quinolones.An Improved Preparation of Intermediates for Novel Potenet Tricyclic Quinolone Antibacterial Agents
David Barrett, Hiroshi Sasaki, Hideo Thuthumi, Takayoshi Kinoshita, and Kazuo Sakane
Bull. Chem. Soc. Jpn. **69**, 1371-1376, (1996)

8) A Novel Synthesis of the Pyrazolo[1,5-a]quinoline Ring System. New N1-C2 Bridged DNA Gyrase Inhibitors via a Novel Tandem 1,4-Conjugate Addition-Michael [3+2] Annulation Process
David Barrett, Hiroshi Sasaki, Takayoshi Kinoshita, Akihiko Fujikawa, and Kazuo Sakane
Tetrahedron **52**, 8471-8488, (1996)

9) Unexpectically facile racemization of 8-diphenylphosphinoyl-8'-methoxy-1.1'-binaphthyl
Kaoru Fuji, Minoru Sakurai, Naoji Tohkai, Akio Kuroda, Takeo Kawabata, Yoshimasa Fukazawa, Takayoshi Kinoshita, and Toshiji Tada
Chem. Commun., 1609-1610, (1996)

10) Structure of the Zinc Endoprotease from *Streptomyces caespitosus*
Genji Kurisu, Takayoshi Kinoshita, Akiko Sugimoto, Akinobu Nagara, Yasushi Kai, Nobutami Kasai, and Shigeharu Harada
J. Biochem. **121**, 304-308, (1997)

11) Assessment of the Activity of 8-Diphenylphoosphosphino-8'-mothoxy-1,1'-binaphthyl as a Ligand for Palladium-Catalyzed Reactions
Kaoru Fuji, Minoru Sakurai, Takayoshi Kinoshita, Toshiji Tada, Akio Kuroda, and Takeo Kawabata
Chemical and Pharmaceutical Bulletin **45**, 1524-1526, (1997)

12) Synthesis, X-ray Crystal Structure, and Biological Activity of FR186054, a Novel, Potent, Orally Active Inhibitor of Acyl-CoA:Cholesterol O-Acyltransferase (ACAT) Bearing a Pyrazol Ring
Akira Tanaka, Takeshi Terasawa, Hiroyuki Hagihara, Takayoshi Kinoshita, Yuri Sakuma, Noriko Ishibe, Masae Sawada, Hisashi Takasugi, and Hirokazu Tanaka
Bioorganic and Medicinal Chemistry Leters **8**, 81-86, (1998)

13) The first synthesis of an optically active molecular bevel gear with only two cogs on each wheel
Kaoru Fuji, Takahiro Oka, Takeo Kawabata, and Takayoshi Kinoshita
Tetrahedron Letters **39**, 1373-1376, (1998)

14) Stepwise construction of some hexahomooxacalix[3]arenes and their conformations in solid state
Kazunori Tsubaki, Tadamune Otsubo, KIyoshi Tanaka, Kaoru Fuji, and Takayoshi Kinoshita
The Journal of Organic Chemistry **63**, 3260-3265, (1998)

15) Complexation of C60 with hexahomooxacalix[3]arenes and supramolecular structures of complexes in the solid state
Kazunori Tsubaki, Kiyoshi Tanaka, Takayoshi Kinoshita, and Kaoru Fuji
Chem. Commun, 895-896, (1998)

16) Palladium-catalyzed asymmetric reduction of allylic esters with a new chiral monodentate ligand, 8-diphenylphosphino-8'-mothoxy-1,1'-binaphthyl
Kaoru Fuji, Minoru Sakurai, Takayoshi Kinoshita, and Takeo Kawabata
Tetrahedron Letters **39**, 6323-6326, (1998)

17) Discovery of 6-oxo-3-(2-phenylpyrazolo[1,5alfa]pyridin-3-yl)-1(6H)-pyridazine -butanoic acid (FK838) : A novel non-xanthine adenosine A1 receptor antagonist with potent diruretic activity
Atsushi Akahane, Hirohito Katayama, Takafumi Mitsunaga, Takeshi Kato, Takayoshi Kinoshita, Yasuhiro Kita, Takahiro Kusunoki, Takao Terai, Keizo Yoshida, and you chi Shiokawa
Journal of Medicinal Chemistry **42**, 779-783, (1999)

18) Visualization of Molecular Length of a,w-Diamines and Temperature by a Receptor Based on Phenolphthalein and Crown Ether
Kaoru Fuji, Kazunori Tsubaki, Kiyoshi Tanaka, Noriyuki Hayashi, Tadamune Otsubo, and Takayoshi Kinoshita
J. Am. Chem. Soc. **121**, 3807-3808, (1999)

19) Discovery of FR166124, a Novel Water-Soluble Pyrazolo-[1,5-a]Pyridine Adenosine A1 Receptor Antagonist
Satoru Kuroda, Atsushi Akahane, Hiromichi Itani, Shintaro Nishimura, Kieran Durkin, Takayoshi Kinoshita, Yoshiyuki Tenda, and Kazuo Sakane
Bioorg. Med. Chem. Lett. **9**, 1979-1984, (1999)

20) Synthesis of the Water-Soluble Adenosine A1 Receptor Antagonist FR166124 Through a Novel Sequential Horner-Emmons/Isomerization Reaction
Satoru Kuroda, Atsushi Akahane, Hiromichi Itani, Shintaro Nishimura, Kieran Durkin, Takayoshi Kinoshita, and Kazuo Sakane
Tetrahedron **55**, 10351-10364, (1999)

21) Molecular Structure of FR901277, A Novel Inhibitor of Human Leukocyte Elastase, and its Binding Mode Simulation
Isao Nakanishi, Takayoshi Kinoshita, Toshiji Tada, Takashi Fujita, Hiroshi Hatanaka, and Akihiro Sato
Bioorg. Med. Chem. Lett. **9**, 2397-2402, (1999)

22) The Supramolecular Structure of 1,4-Bis(9-fluorenyl)-1,4-dihydro[60]fullerene with Hexahomotrioxacalix[3]arene in the Solid State
Kazunori Tsubaki, Yasujiro Murata, Koichi Komatsu, Takayoshi Kinoshita, and Kaoru Fuji
Heterocycles **51**, 2553-2556, (1999)

23) A New Antimitotic Substance, FR182877
Seiji Yoshimura, Bunji Sato, Takayoshi Kinoshita, Shigehiro Takase, and Hiroshi Terano
The Journal of Antibiotics **53**, 615-622, (2000)

24) Structure of porcine pancreatic elastase complexed with FR901277, a novel macrocyclic inhibitor of elastases, at 1.6 A resolution
Isao Nakanishi, Takayoshi Kinoshita, Akihiro Sato, and Toshiji Tada
Biopolymers **53**, 434-445, (2000)

25) Stereoselective Synthesis of CF2-Substituted Phosphothreonine Mimetics and Their Incorporation into Peptides Using Newly Developed Deprotection Procedures
Akira Otaka, Etsuko Mitsuyama, Takayoshi Kinoshita, Hirokazu Tamamura, and Nobutaka Fujii
J. Org. Chem. **65**, 4888-4899, (2000)

26) Recognition of the chain length of a,w-diamines by a meso-ternaphthalene derivative with two crown ethers
Kazunori Tsubaki, Hiroyuki Tanaka, Takumi Furuta, Takayoshi Kinoshita, and Kaoru Fuji
Tetrahedron Letters **41**, 6089-6093, (2000)

27) Memory of Chirality in Diastereoselective α-Alkylation of Isoleucine and allo-Isoleucine Derivatives
Takeo Kawabata, Jianyong Chen, Hideo Suzuki, Yoshikazu Nagae, Takayoshi Kinoshita, Sirirat Chancharunee, and Kaoru Fuji
Organic Letters **2**, 3883-3885, (2000)

28) The first example for cycloenatiomeric hexahomooxacalix[3]arenes
Kazunori Tsubaki, Tadamune Otsubo, Takayoshi Kinoshita, Mitsuru Kawada, and Kaoru Fuji
Chem. Pharm. Bull. **49**, 507-509, (2001)

29) Synthesis, Structure, and Ion-binding Properties of New Tetraoxacalix[3]arenes
Kazunori Tsubaki, Tetsuya Morimoto, Tadamune Otsubo, Takayoshi Kinoshita, and Kaoru Fuji
J. of Org. Chem. **66**, 4083-4086, (2001)

30) Purification, Crystallization and preliminary X-ray diffraction analysis of the fructose-1,6/sedoheptulose-1,7-bisphosphatase of Synechococcus PCC 7942
Yoshihiro Nakamura, Toshiji Tada, Kei Wada, Takayoshi Kinoshita, Masahiro Tamoi, Shigeru Shigeoka, and Keiichiro Nishimura
Acta Cryst. **D57**, 454-456, (2001)

31) Crystallization and preliminary X-ray diffraction analysis of NADP-dependent glyceraldehide-3-dehydrogenase of Synechococcus PCC 7942
Yoshihiro Nakamura, Toshiji Tada, Kei Wada, Takayoshi Kinoshita, Masahiro Tamoi, Shigeru Shigeoka, and Keiichiro Nishimura
Acta Cryst. **D57**, 879-881, (2001)

32) Crystallization and Preliminary X-ray diffraction studies of catalase-peroxidase from Synechococcus PCC 7942
Kei Wada, Toshiji Tada, Yoshihiro Nakamura, Takayoshi Kinoshita, Masahiro Tamoi, Shigeru Shigeoka, and Keiichiro Nishimura
Acta Cryst. **D58**, 157-159, (2002)

33) Synthesis of the proton-ionizable lariat crown ether and chiral recognition of primary amines
Kazunori Tsubaki, Hiroyuki Tanaka, Takayoshi Kinoshita and Kaoru Fuji
Tetrahedron **58**, 1679-1684, (2002)

34) Use of meso-ternaphthalene derivatives: linear recognition of the a,w-diamines by homoditopic receptorsSynthesis of the proton-ionizable lariat crown ether and chiral recognition of primary amines
Kazunori Tsubaki, Hiroyuki Tanaka, Takumi Furuta, Kiyoshi Tanaka, Takayoshi Kinoshita and Kaoru Fuji
Tetrahedron **58**, 5611-5617, (2002)

35) Regio- and Stereoselective Synthesis of (E)-Alkene trans-Xaa-Pro Dipeptide Mimetics Utilizing Organocopper-Mediated Anti-Sn2' Reactions
Akira Otaka, Fumihiko Katagiri, Takayoshi Kinoshita, Yoshihiko Odagaki, Oishi Shinya, Hirokazu Tamamura, Nobuyuki Hamanaka and Nobutaka Fujii
J. Org. Chem. **67**, 6152-6161, (2002)

36) Enantiometric Recognition of Amino Acids Using a Chiral Spiropyran Derivative
Kazunori Tsubaki, Koichiro Mukoyoshi, Hiroshi Morikawa, Takayoshi Kinoshita and Kaoru Fuji
Chirality 14, 713-715, (2002)